lene glycol-*bis*(2-aminoethyl)-*N,N,N,N*-tetraacetic acid (EGTA) (Ca^{2+}-free BSS).

Construction of Lentivirus Vectors Expressing Interfering Short Hairpin RNA (shRNAi) and Microglial Transduction

Lentivirus containing shRNAi was prepared by the method previously described (Yogosawa et al., 2005). The self-inactivating (SIN) vector construct pCS-RfA-CG, which contains the EGFP gene under the control of the CMV promoter and sites for site-specific recombination with a Gateway vector (attR1,2), was used for simultaneous expression of EGFP and shRNA. Plasmid containing $P2X_4R$ shRNAi under the control of human U6 promoter was provided by Dr. K. Inoue (Kyushu Univ. Fukuoka, Japan). The gene of the $P2X_4R$ shRNAi-expressing cassette inserted into pENTR™1A was transferred into the pCS-RfA-CG by a recombination reaction using Gateway LR Clonase (Invitrogen). The sequence of shRNA targeted for firefly luciferase was used as a control (Nishitsuji et al., 2004). The sequence was inserted into the piGENE™ hU6 *Bsp*MI vector (iGENE Therapeutics, Tsukuba, Japan), and the gene of the luciferase shRNAi-expressing cassette was ligated into the pCS-RfA-CG. The sequence of $shP2X_4R$ was: 5′-GGG ATA AGA GAT ATA GGT AAC GTG TGC TGT CCG TTA CTT ATA TTT CTT GTC CCT TTT T-3′. We confirmed the specificity of P2×4R shRNAi by a coexpression assay. pCS-shP2×4R-CG was cotransfected into Cos7 cells with P2×4 expression plasmid (provided by Dr. K. Inoue) or HA-tagged P2Y12R plasmid (Supplemental information). pCS-shP2×4R-CG significantly suppressed P2×4R expression but had no effect P2Y12R expression. The recombined plasmid was cotransfected into 293FT cells (Invitrogen) with a packaging plasmid (pCAG-HIVgp) and a plasmid expressing Rev and vesicular stomatitis virus G glycoprotein (pCMV-VSV-G-RSV-Rev), and the supernatant was collected after 48 h and filtered through a 0.45-μm pore filter (Falcon). Viral particles in the supernatant were concentrated by ultracentrifugation for 2 h at 19,400 rpm (SW28 rotor; Beckmann Coulter, CA) and recovered by suspension in Hanks buffered saline (Invitrogen).

The recombinant lentivirus (2×10^5 infectious units) was added to the mixed glial cells that had been cultured for 12 days in a 25-cm^2 flask, and cultured for 6 days in DMEM containing 10% FCS. Floating cells were collected as microglia and allowed to attach to appropriate dishes or glasses. The efficiency of microglia transduction with the $shP2X_4R$ vector was 20–30%, the same as with the shControl vector according to an analysis of the number of microglia expressing EGFP by flow cytometry.

Isolation of EGFP-Positive Microglia

After transduction with the lentivirus vectors, floating cells collected as microglia were resuspended in PBS containing 2% FCS. EGFP-positive and -negative cells were sorted with a FACSVantageSE flow cytometry system (BD Biosciences). Live gating was performed with propidium iodide (Sigma-Aldrich, St. Louis, MO). The purity of the EGFP-positive cells was >99% according to a flow cytometry analysis.

Western Blot Analysis of P2X Receptor Expression

Sorted cells were lysed in SDS sample buffer. $P2X_4R$, $P2X_7R$, EGFP, and actin proteins in the lysate equivalent to 2×10^4 cells were separated by 10% SDS-PAGE and detected by Western blot analysis with 1 μg/mL anti-$P2X_4R$ antibody (Alomone Labs, Jerusalem, Israel), 0.6 μg/mL anti-$P2X_7R$ (Alomone Labs), anti-GFP antibody (diluted 1:1,000, Medical & Biological Laboratories, Nagoya, Japan), and anti-actin antibody (diluted 1:1,000, Sigma), respectively, and visualized with the ECL system.

RT-PCR Analysis for $P2Y_{12}R$ Gene Transcripts

RNA was isolated from the sorted cells with the RNeasy Mini Kit (QIAGEN, Hildem, Germany) containing a DNase treatment, according to the manufacturer's protocols. Reverse transcription of RNA was performed with SuperScript III reverse transcriptase (Invitrogen). The PCR amplification conditions were 30 s at 94°C, 15 s at 60°C, and 30 s at 68°C for 25–35 cycles, except for the initial denaturation step of 2 min at 94°C and the final cycle with an elongation step of 5 min at 68°C. An extra reaction mixture without reverse transcriptase was used as a control for DNA contamination of the RNA sample. The primers used were as follows: rat $P2Y_{12}R$, 5′-AAA CTT CCA GCC CCA GCA ATC T-3′ (forward), 5′-CAA GGC AGG CGT TCA AGG AC-3′ (reverse); rat β-actin, as an internal standard, 5′-TTG TTA CCA ACT GGG ACG ACA TGG-3′ (forward), 5′-GAT CTT GAT CTT CAT GGT GCT AGG-3′ (reverse). PCR products of 447 bp for $P2Y_{12}R$ and 763 bp for β-actin were analyzed on a 1.5% agarose and stained with ethidium bromide. The relative intensity of the bands for $P2Y_{12}R$ was quantified by densitometry with NIH image software and normalized to the β-actin products. The normalized values were used to calculate the ratio of $P2Y_{12}R$ mRNA level in the EGFP-positive cells transduced with the $shP2X_4R$ vector to the level in the EGFP-positive cells transduced with the shControl vector.

Calcium Imaging

The intracellular calcium concentration ($[Ca^{2+}]_i$) was monitored by the fura-2 method described by Inoue et al. (1998), using a highly sensitive intensifier target video camera C2400 and an Argus 50 image processor (Hama-

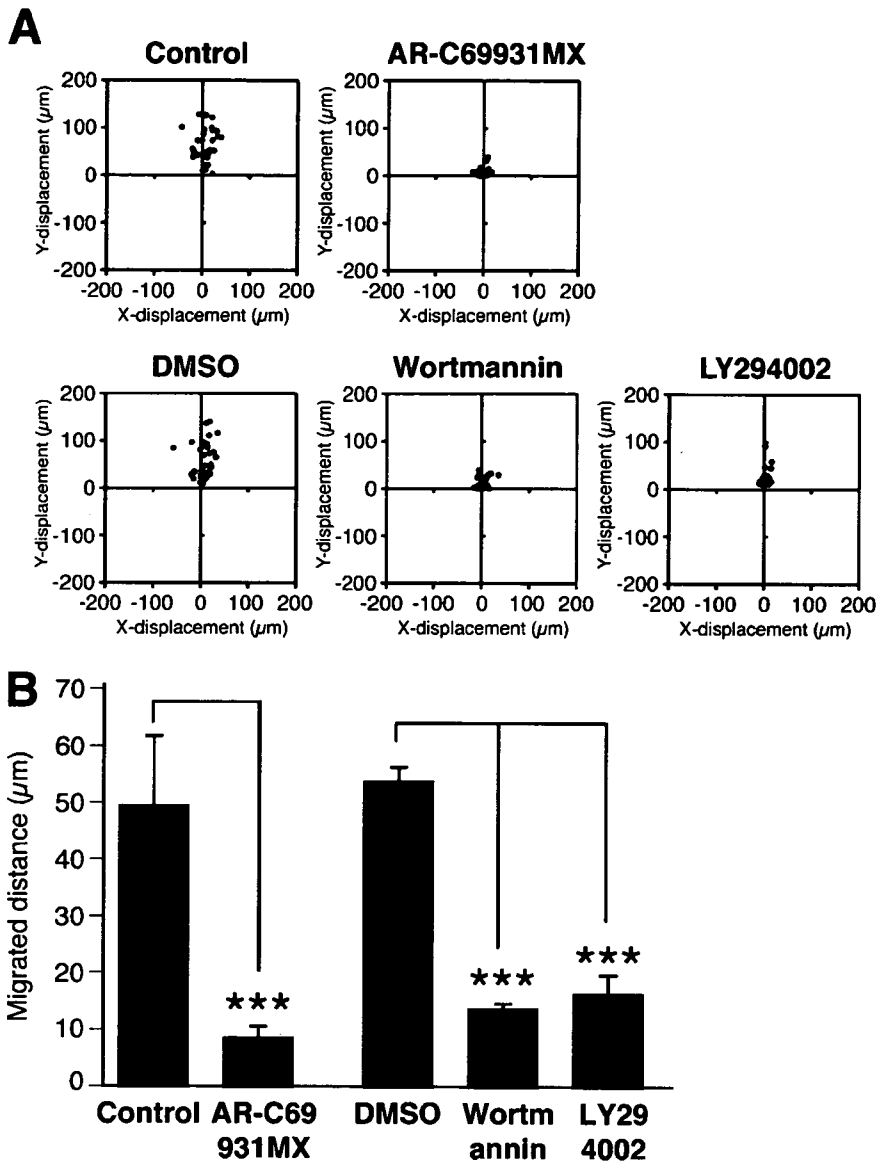

Fig. 1. Effect of PI3K inhibitors on ATP-induced microglial chemotaxis. (**A**) Microglia were pretreated with 1 μM AR-C69931MX for 10 min or with 0.125% DMSO, 100 nM wortmannin, or 50 μM LY294002 for 20 min, and microglial migration towards 50 μM ATP was observed in the Dunn chemotaxis chamber. The distance and direction migrated by individual cells are shown as x and y coordinates on scatter diagrams. The position of the outer well of the chamber is at the top in the vector diagrams of cells. (**B**) Chemotaxis by each cell was quantified by measuring the (x, y) distance migrated from the starting position. Data are means ± SD of three independent experiments. $^{***}P < 0.001$, Student's t-test.

matsu Photonics). Microglia transduced with the lentivirus vectors were plated at 2×10^5 cells/well on poly-L-lysine-coated CELLocate microgrid coverslips (Eppendorf, Hambrug, Germany). After 2 h, the cells were incubated with 10 μM fura-2 acetoxymethylester (fura-2/AM, Dojindo Laboratories, Kumamoto, Japan) at 37°C for 30 min in DMEM containing 25 mM HEPES (DMEM-H, Invitrogen), and the coverslips were mounted on an inverted epifluorescence microscope (TMD-300, Nikon, Tokyo, Japan). The cells were exposed to drugs dissolved in DMEM-H by superfusion. Raw data were recorded as 500-nm emissions of fura-2 excited alternately at 340 and 380 nm, and $[Ca^{2+}]_i$ was expressed as the ratio of the fluorescence intensity at 340 nm to the fluorescence intensity at 380 nm (F340/380).

RESULTS

Involvement of the PI3K Pathway in ATP-Induced Microglial Chemotaxis

We previously reported that ATP-induced microglial membrane ruffling were inhibited by treatment with pertussis toxin and a P2Y$_{12}$R-selective antagonist, AR-C69931MX, suggesting that Gi/o-coupled P2Y$_{12}$R is involved in both the membrane ruffling and the chemotaxis (Honda et al., 2001). Stimulation of P2Y$_{12}$R has been reported to induce PI3K activation (Czajkowski et al., 2004; Soulet et al., 2004; Van Kolen and Slegers, 2004). To determine whether PI3K activation is required for chemotaxis by ATP-stimulated microglia, we investigated the effects of the PI3K inhibitors wortmannin and

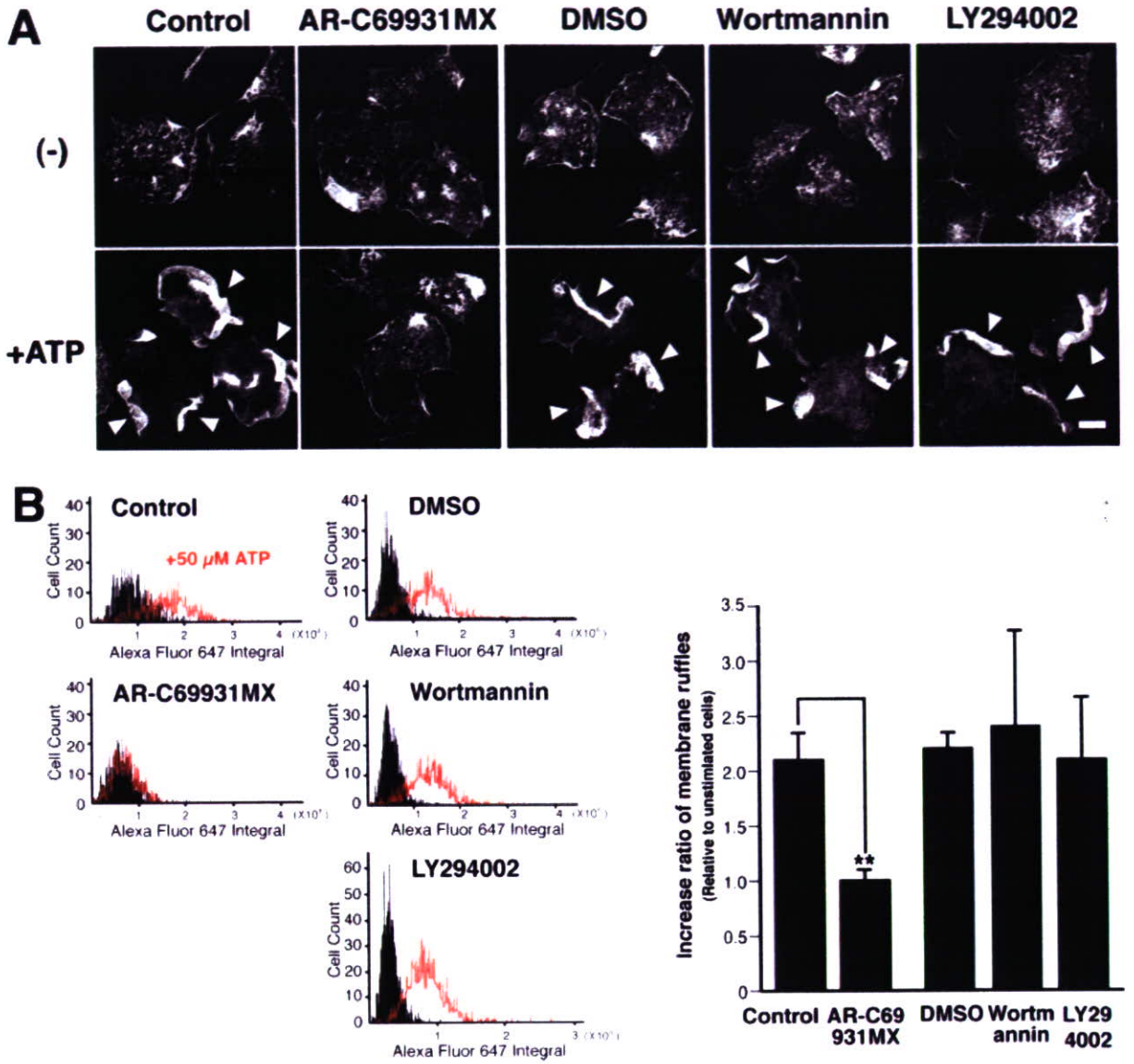

Fig. 2. Effect of PI3K inhibitors on ATP-induced microglial membrane ruffling. (**A**) Microglia were pretreated with 1 μM AR-C69931MX, 0.125% DMSO, 100 nM wortmannin, or 50 μM LY294002 as described in Fig. 1A, and then stimulated with 50 μM ATP for 5 min. After fixation, the cells were stained with Texas Red-conjugated phalloidin to visualize membrane ruffles. Arrowheads indicate membrane ruffles. Scale bar, 10 μm. (**B**) Quantification of membrane ruffles. Microglia were stimulated as in A for 5 min, fixed, and stained with an anti-Iba1 antibody and Alexa Fluor 647-conjugated phalloidin to recognize individual microglial cells and membrane ruffles, respectively. The F-actin content of microglial cells was quantified as integral intensity of Alexa Fluor 647 fluorescence by using LSC. The five panels on the left side are histograms representing the total F-actin in each cell (x-axis, Alexa fluor 647 integral) and the number of scanned cells (y-axis, cell count). The black region represents the unstimulated cells, and the region surrounded by the red line represents the ATP-stimulated cells. The bar graph on the right side shows the ratio of the mean of fluorescent intensity of ATP-stimulated cells to that of unstimulated cells after treatment with each inhibitor. Data are means ± SD of three independent experiments. $^{**}P < 0.01$, Student's t-test.

LY294002 with a Dunn chemotaxis chamber. Microglial chemotaxis toward the higher concentration of ATP was evaluated by analysis of time-lapse images. When 50 μM ATP was applied to the outer well, the cells migrated toward higher concentrations of ATP. Pretreatment of the microglia with wortmannin or LY294002 significantly blocked the chemotaxis (Fig. 1A). The chemotactic movement of the microglia was quantified by calculating the (x, y) distances individual cells migrated toward ATP. As shown in Fig. 1B, the mean distance migrated by cells pretreated with PI3K inhibitors was significantly shorter than the distance migrated by cells pretreated with DMSO. Treatment with 1 μM AR-C69931MX also inhibited the chemotaxis, as expected based on the results of our previous study (Honda et al., 2001). These findings suggested that PI3K activation is necessary for ATP-induced microglial chemotaxis.

Next, we investigated the effect of PI3K inhibitors on ATP-induced microglial membrane ruffling. As shown in Fig. 2A, phalloidin staining clearly demonstrated that ATP stimulation caused membrane ruffling within 5 min. Pretreatment of microglia with AR-C69931MX inhibited the ATP-induced membrane ruffling, as reported previously (Honda et al., 2001). However, exposure to 100 nM wortmannin or 50 μM LY294002 appeared to have no effect on the membrane ruffling. To confirm the effect of PI3K inhibitors on membrane ruffling quantitatively, the increase in F-actin in cells with membrane ruffles was analyzed with a laser scanning cytometer (LSC), which is a microscope-based cytometer. ATP-stimulated and unstimulated cells were stained with an anti-Iba1 antibody and Alexa Fluor 647-conjugatde phalloidin, and F-actin content was quantified by calculating the mean Alexa Fluor 647 fluorescent intensity of individual cells positive for a microglial marker protein Iba1 (Ito et al., 1998). As shown in Fig. 2B, the mean fluorescent intensity of control microglia was increased approximately 2-fold by ATP stimulation. The fluorescent intensity of ATP-stimulated cells pretreated with AR-C69931MX did not change significantly; however, the fluorescent intensity of cells pretreated with wortmannin or LY294002 was increased by ATP stimulation the same as in the control and the DMSO-treated cells. These results indicate that PI3K activation is not required for the membrane ruffling, but is necessary for induction of microglial chemotaxis.

ATP-Induced Akt Phosphorylation and Effect of Extracellular Calcium Deprivation

To determine whether the PI3K pathway in microglia is activated by ATP stimulation, we investigated Akt phosphorylation, a downstream signaling for PI3K (Bellacosa et al., 1991; Scheid and Woodgett, 2003), by Western blot analysis with a phospho-specific Akt antibody. ATP stimulation rapidly increased the level of Akt phosphorylation in a time-dependent manner (Fig. 3A), and pretreatment with 1 μM AR-C69931MX or 100 nM wortmannin inhibited the increase in Akt phosphorylation (Figs. 3B,C). These results indicated that ATP induces activation of the PI3K/Akt cascade in microglia and that the activation is mediated by P2Y$_{12}$R.

Previous studies (Inoue et al., 1998; Tsuda et al., 2003) have shown that stimulation of microglia with 50 μM ATP induces a transient increase in $[Ca^{2+}]_i$ that depends on the presence of extracellular Ca^{2+}, suggesting that ionotropic P2X receptors are responsible for the Ca^{2+} response. Use of the Ca^{2+}-sensitive fluorescent dye fura-2 revealed that the chelation of extracellular Ca^{2+} suppressed the ATP (50 μM)-evoked increase in $[Ca^{2+}]_i$ in our cultured microglia (data not shown). To determine whether the increase in $[Ca^{2+}]_i$ had any effect on the PI3K/Akt activation, we investigated Akt phosphorylation in microglia stimulated with 50 μM ATP in the absence of extracellular Ca^{2+}, and as shown in Fig. 4, chelation of extracellular Ca^{2+} by EGTA significantly

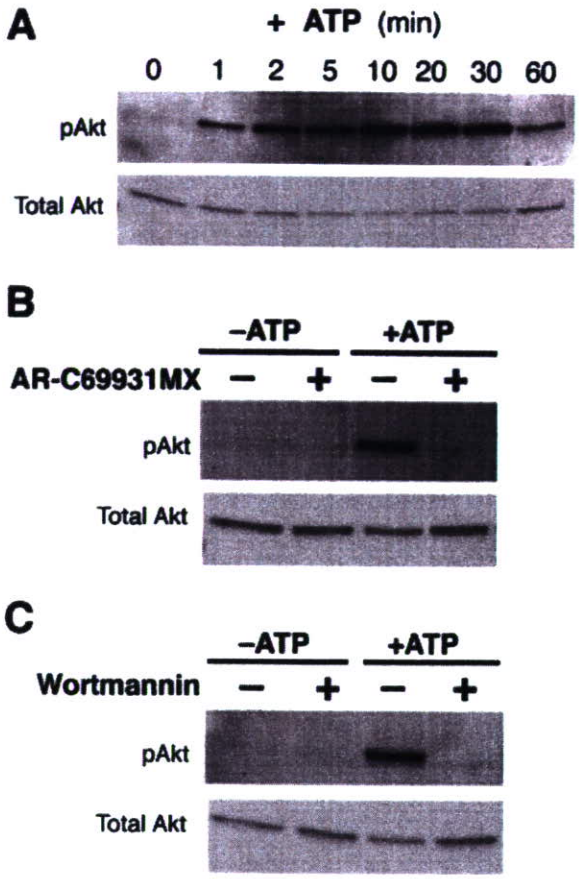

Fig. 3. ATP-induced Akt phosphorylation in microglia is dependent on PI3K activation through P2Y$_{12}$R. (**A**) Microglia were stimulated with 50 μM ATP for the period of time indicated and then lysed in SDS sample buffer. Phosphorylated (pAkt) and total Akt in the lysates were detected by Western blot analysis. (**B**, **C**) Microglia were pretreated with 1 μM AR-C69931MX for 10 min (**B**) or with 100 nM wortmannin for 20 min (**C**) and then stimulated with 50 μM ATP for 5 min. Akt phosphorylation was detected by Western blot analysis. Similar results were obtained from three independent experiments.

decreased ATP-induced Akt phosphorylation. Previous studies have shown that M-CSF stimulates the Fms tyrosine kinase receptor to activate Akt in macrophages in a PI3K-dependent manner (Comalada et al., 2004; Weiss-Haljiti et al., 2004). M-CSF also stimulated Akt phosphorylation in microglia, but chelation of extracellular Ca^{2+} had no effect on it (Fig. 4). These results led us to speculate that the ATP-induced PI3K/Akt activation, which is an essential component for induction of microglial chemotaxis, was linked to an increase in $[Ca^{2+}]_i$ through the extracellular Ca^{2+}-influx via ionotropic P2X receptors.

Effect of P2XR Antagonists on ATP-Induced Microglial Chemotaxis and Akt Phosphorylation

Since primary-cultured microglia have been shown to express P2X$_4$R (Tsuda et al., 2003; Xiang and Burnstock,

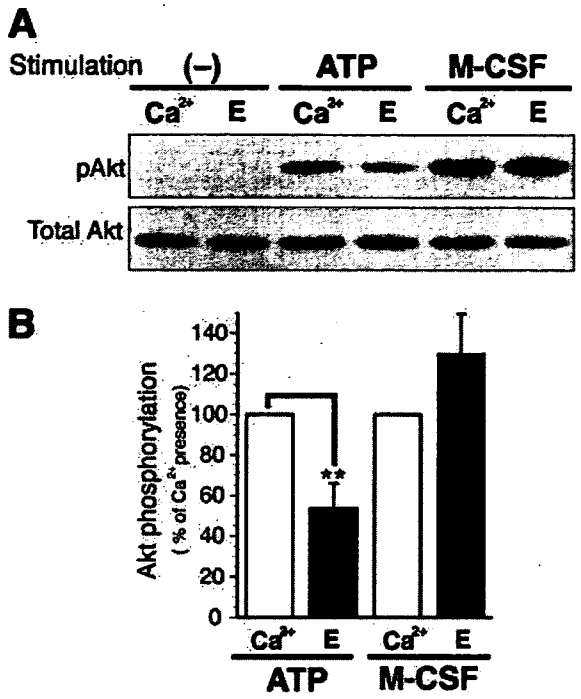

Fig. 4. Inhibitory effect of chelation of extracellular calcium on ATP-stimulated Akt phosphorylation. (**A**) Microglia were incubated for 30 min in BSS containing 1.2 mM Ca^{2+} (Ca^{2+}) or 1 mM EGTA (E) and then stimulated with 50 μM ATP or 100 ng/mL M-CSF for 5 min. Akt phosphorylation was detected by Western blot analysis. (**B**) The Akt phosphorylation level was quantified by densitometry. The results are expressed as percentage of agonist-induced phosphorylation in the presence of Ca^{2+} and are means ± SD of three independent experiments. $^{**}P < 0.01$; Student's *t*-test.

2005) and $P2X_7R$ (Ferrari et al., 1996; Nörenberg et al., 1994; Verkhratsky and Kettenmann, 1996; Walz et al., 1993), we first investigated the involvement of P2XRs in microglial chemotaxis with a $P2X_{1-4}R$, antagonist TNP-ATP, with a $P2X_{1,2,3,5,7}R$ antagonist PPADS, and with a selective $P2X_7R$ antagonist BBG. After pretreatment with an antagonist for 5 min the microglia were observed for chemotactic movement toward ATP in a Dunn chemotaxis chamber containing the antagonist. Treatment with 100 μM TNP-ATP appeared to suppress the ATP-induced microglial chemotaxis, but 300 μM PPADS or 1 μM BBG had no effect (Fig. 5A). The chemotactic movement of the microglia was quantified by calculating the mean value of the total (x, y) distances of individual cells migrated toward ATP. As shown in Fig. 5B, the mean distance migrated by the cells pretreated with TNP-ATP was significantly shorter than the distance migrated by the control cells, but the values of the cells pretreated with PPADS or BBG were not significantly different from those of the controls. Treatment with 1 μM AR-C69931MX also completely inhibited the chemotaxis. These results suggested that $P2X_4R$ as well as $P2Y_{12}R$ is involved in ATP-induced microglial chemotaxis.

We next examined the effect of the three P2XR antagonists, TNP-ATP, PPADS, and BBG, on ATP-stimulated Akt phosphorylation. TNP-ATP significantly suppressed the ATP-stimulated Akt phosphorylation, but PPADS or BBG appeared to have no effect (Fig. 6). AR-C69931MX also completely inhibited Akt phosphorylation. These results suggested that ATP-induced PI3K/Akt activation is mediated by $P2X_4R$ as well as $P2Y_{12}R$.

Downregulation of $P2X_4R$ in Microglia by Short Hairpin $P2X_4R$ RNAi

To determine whether $P2X_4R$ is in fact involved in ATP-induced microglial chemotaxis, we suppressed $P2X_4R$ expression in microglia with RNAi. We constructed a lentivirus vector that expresses both short hairpin (sh)-RNAi and EGFP under the control of the U6 RNA polymerase III promoter and the CMV promoter, respectively (Fig. 7A), and thus cells expressing the shRNAi should also express the EGFP reporter. Microglia were transduced with a lentivirus vector expressing a short hairpin $P2X_4R$ RNAi ($shP2X_4R$) or a control vector that expressed short hairpin luciferase RNAi (shControl). Lentiviral particles were added to mixed glial cell cultures, and floating cells were collected as microglia. To confirm the suppression of $P2X_4R$ expression by $shP2X_4R$, EGFP-positive cells were sorted with a flow cytometer, and expression of $P2X_4R$ protein in the cell lysate was investigated by Western blot analysis with an anti-$P2X_4R$ antibody. $P2X_4R$ protein expression was markedly suppressed in the EGFP-positive cells transduced with $shP2X_4R$ (Fig. 7B), whereas there was no difference in $P2X_4R$ protein level between the EGFP-positive and EGFP-negative cells after transduction with shControl. $P2X_7R$ protein expression was unaffected by transduction with $shP2X_4R$ (Fig. 7B). Microglial RNA was isolated from the sorted cells, and $P2Y_{12}R$ mRNA levels were analyzed by RT-PCR and normalized against actin mRNA levels. $P2Y_{12}R$ mRNA levels increased linearly with PCR reactions for 25–35 cycles. When PCR reactions were performed for 27 cycles, there was no difference in relative level of $P2Y_{12}R$ mRNA in EGFP-positive cells between transduction with $shP2X_4R$ and transduction with shControl (ratio of $P2Y_{12}R$ mRNA level in the $shP2X_4R$-transduced cells to the shControl-transduced cells = 1.1, Fig. 7C). We checked the $P2Y_{12}R$ mRNA level amplified by PCR for 25 and 30 cycles and confirmed that the relative level of $P2Y_{12}R$ mRNA in the $shP2X_4R$-transduced cells was the same as in the shControl-transduced cells. These results indicated that $P2X_4R$ expression was specifically suppressed in the EGFP-positive microglia after transduction with $shP2X_4R$.

The increase in $[Ca^{2+}]_i$ induced by ATP (50 μM) in microglia has been shown to be mediated by $P2X_4R$ (Tsuda et al., 2003). To determine whether $shP2X_4R$ interfered with $P2X_4R$ function in the EGFP-positive microglia, the level of $[Ca^{2+}]_i$ in individual cells was monitored by imaging analysis with fura-2 after transduction with the lentivirus vectors. A 30-s application of 50 μM ATP produced an increase in the 340/380 emission ratio of fura-2 in the EGFP-positive cells transduced with the con-

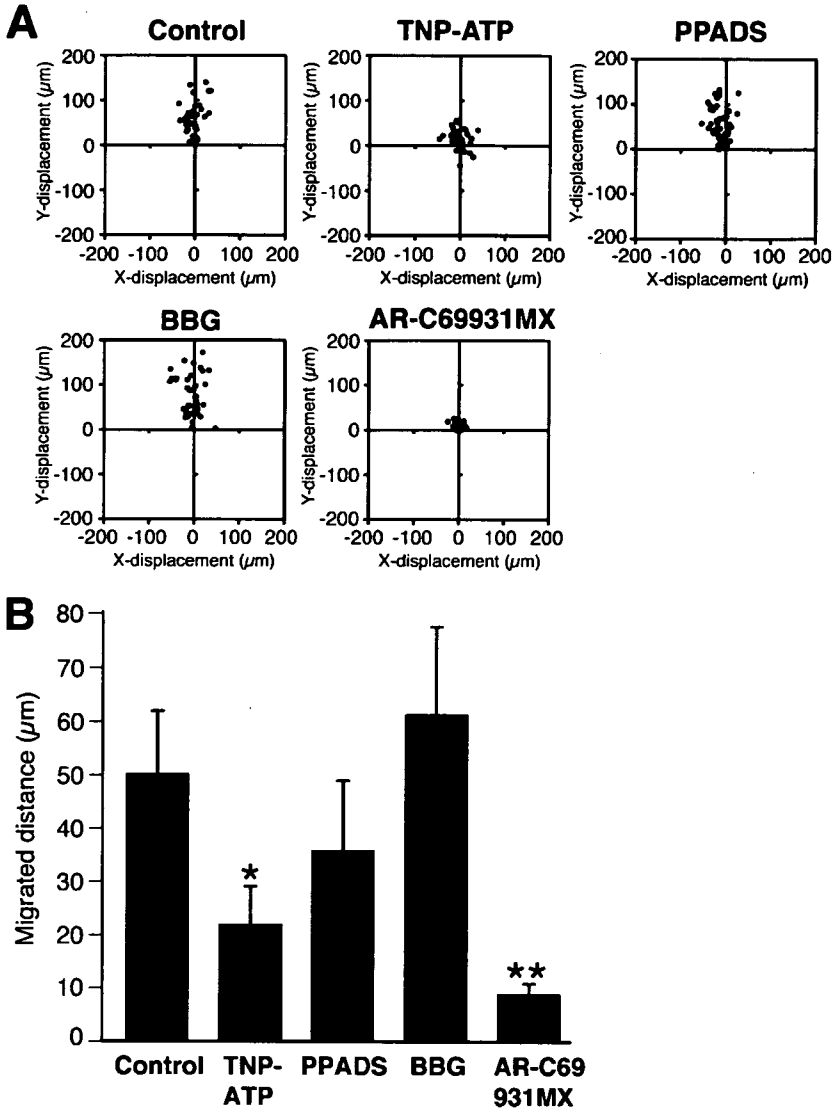

Fig. 5. Effect of P2X antagonists on ATP-induced microglial chemotaxis. (**A**) Microglia were pretreated with 100 μM TNP-ATP, 300 μM PPADS, or 1 μM BBG for 5 min or with 1 μM AR-C69931MX for 10 min. Microglial migration towards 50 μM ATP was observed in the Dunn chemotaxis chamber. The distance and direction of migration by individual cells are shown as x and y coordinates on scatter diagrams. (**B**) Chemotaxis was quantified by measuring the (x, y) distance migrated from the starting position of cells. Data are means ± SD of three independent experiments. $^{*}P < 0.05$, $^{**}P < 0.01$, Student's t-test.

trol vector (Fig. 8A left), whereas the increase in 340/380 emission ratio was significantly attenuated in the EGFP-positive cells transduced with shP2X$_4$R (Figs. 8A,B). These results confirmed that transduction with shP2X$_4$R downregulates expression of P2X$_4$R protein.

Effect of shP2X$_4$R on ATP-Induced Membrane Ruffling and Chemotaxis by Microglia

The effect of P2X$_4$R downregulation on ATP-induced membrane ruffling was examined in microglia transduced with the lentivirus vectors. EGFP-positive cells transduced with shP2X$_4$R or shControl developed membrane ruffles in response to ATP stimulation, the same as EGFP-negative cells (Fig. 9). These results indicated that shP2X$_4$R did not inhibit the activation of P2Y$_{12}$R and suggested that P2X$_4$R downregulation had no effect on ATP-induced membrane ruffling.

The cells transduced with the vectors were also examined for chemotactic movement in a Dunn chemotaxis chamber. As shown in the scatter diagrams, the migration of EGFP-positive cells transduced with shP2X$_4$R (Fig. 10A, bottom left) was clearly inhibited in comparison with the EGFP-negative cells (bottom right). EGFP-positive cells transduced with shControl (top left) migrated toward ATP as same as the EGFP-negative cells (top right). To quantify the effect of the shRNAi on the chemotactic movement of microglia, we calculated the mean value of the (x, y) distances EGFP-positive and -negative cells migrated toward ATP (Fig. 10B). The mean distance migrated by the EGFP-positive cells transduced with shP2X$_4$R was significantly shorter than both the mean distance migrated by the EGFP-negative cells and the mean distance migrated by the EGFP-positive cells

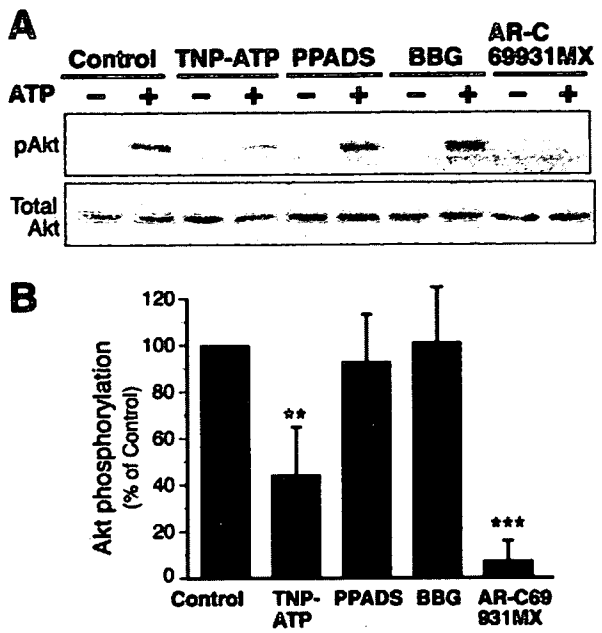

Fig. 6. Effect of P2X antagonists on ATP-stimulated Akt phosphorylation. (A) Microglia were pretreated with 100 μM TNP-ATP, 30 μM PPADS, or 100 nM BBG for 5 min or with 1 μM AR-C69931MX for 10 min, and then stimulated with 50 μM ATP for 5 min. Akt phosphorylation was detected by Western blot analysis. (B) The Akt phosphorylation level was quantified by densitometry and expressed as percentage of ATP-induced phosphorylation in control cells. The data shown are means ± SD of three independent experiments. $^{**}P < 0.01$, $^{***}P < 0.001$; Student's t-test.

transduced with shControl. There was no difference in distance migrated by the EGFP-positive cells and the EGFP-negative cells after transduction with shControl. These results clearly indicated that $P2X_4R$ is involved in ATP-induced microglial chemotaxis.

DISCUSSION

As expected from our previous findings (Honda et al., 2001), both the ATP-induced microglial membrane ruffling and chemotaxis were completely inhibited by a specific $P2Y_{12}R$ antagonist, AR-C69931MX, (Figs. 1 and 2). In this study we further investigated the signaling pathway downstream for $P2Y_{12}R$ and the effect of P2XR antagonists and shRNAi against $P2X_4R$ on microglial migration, and we found that $P2X_4R$ is also involved in ATP-induced microglial chemotaxis.

$P2Y_{12}R$ was known to be coupled to activation of PI3K and inhibition of adenylate cyclase (Czajkowski et al., 2004; Soulet et al., 2004; Van Kolen and Slegers, 2004), and Nasu-Tada et al. (2005) recently reported that a $P2Y_{12}R$-mediated decrease in cyclic AMP is an important step in membrane ruffling and chemotaxis by microglia on fibronectin-coated dishes. PI3K is well known to be a key player in remodeling of the actin cytoskeleton and in regulating cell migration, including chemotaxis (Procko and McColl, 2005; Van Haastert and Devreotes, 2004). In this study we showed that PI3K inhibitors

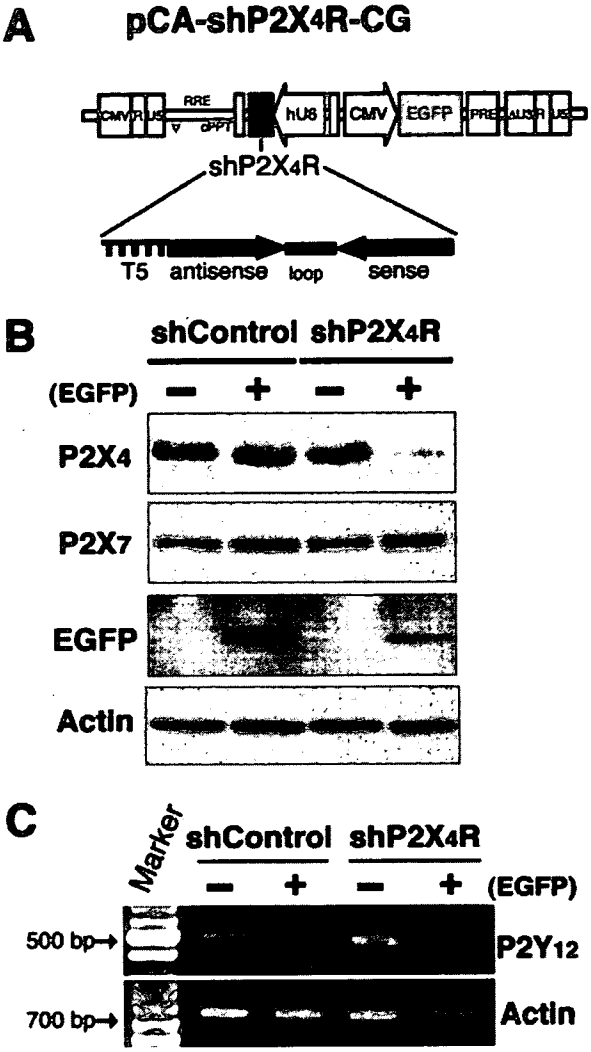

Fig. 7. shRNAi-targeted downregulation of $P2X_4R$ in microglia by lentivirus vectors. (A) Schematic drawing of lentivirus vectors expressing EGFP and shRNAi against $P2X_4R$ ($shP2X_4R$). A shRNA sequence targeted for firefly luciferase (shControl) was used as a control. (B) Protein expression of $P2X_4R$ and $P2X_7R$ in the microglia transduced with the shRNAi lentivirus vectors. EGFP-positive (+) and -negative (−) cells were sorted with a flow cytometer and lysed in SDS sample buffer. Protein expression of $P2X_4R$, $P2X_7R$, EGFP, and actin in the cell lysates was detected by Western blot analysis. Actin served as an internal control. (C) Gene transcript analysis of microglia transduced with the shControl or $shP2X_4R$ vector. RNA was isolated from the sorted cells. Gene transcripts for $P2Y_{12}R$ and β-actin, which served as an internal control, were analyzed by RT-PCR. The relative intensity of the bands for $P2Y_{12}R$ was quantified by densitometry and normalized to the β-actin products. Similar results were obtained from at least three independent experiments.

blocked microglial chemotaxis towards ATP (Fig. 1). However, the PI3K inhibitors had no effect on membrane ruffling (Fig. 2), suggesting that the initial actin reorganization induced by ATP is not dependent on PI3K activation, whereas the ATP gradient-dependent cell migration requires PI3K activation. PI3Ks phosphorylate phosphoinositides at the 3-hydroxyl of the inositol

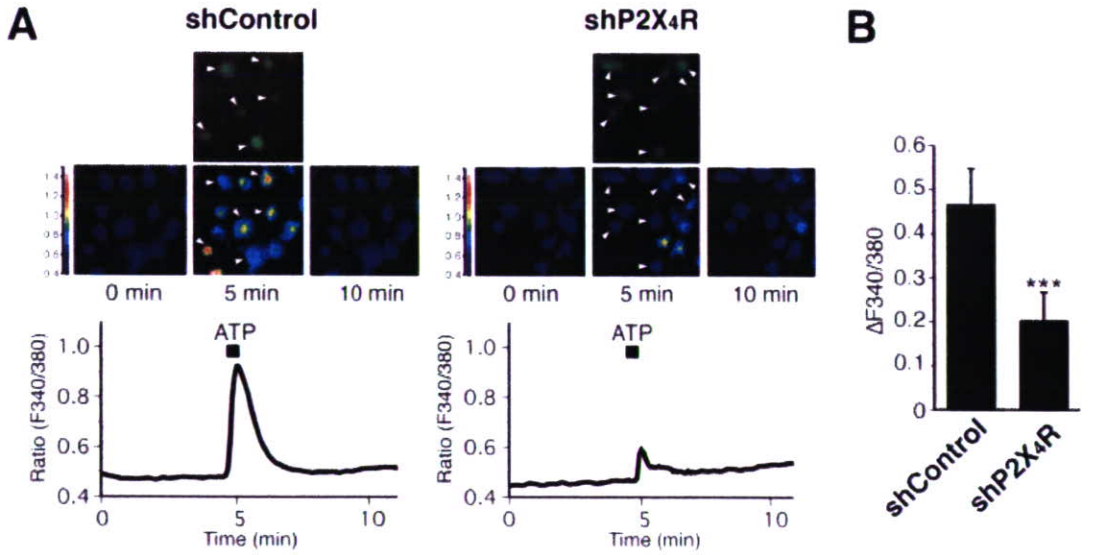

Fig. 8. Effect of P2X$_4$R downregulation on the ATP-evoked increase in $[Ca^{2+}]_i$ in microglia. (**A**) Microglia transduced with the shControl (left panel) or shP2X$_4$R (right panel) vector were loaded with fura-2/AM. $[Ca^{2+}]_i$ was expressed as the ratio of the fluorescence intensity at 340 nm to the fluorescence intensity at 380 nm (F340/380). The pseudocolor image shows three frames (0, 5, and 10 min) of fura2-loaded microglia stimulated with 50 μM ATP for 30 s. Arrowheads point to EGFP-positive cells. The traces show the mean increase in F340/380 emission ratio of 14 EGFP-positive cells from each culture. (**B**) The graphs show the relative increase in ratio (ΔF340/380; mean ± SD, n = 14 cells) from the basal level of the EGFP-positive cells shown in Fig. 8A. $^{***}P < 0.001$; Student's t-test. Similar results were obtained from three independent experiments.

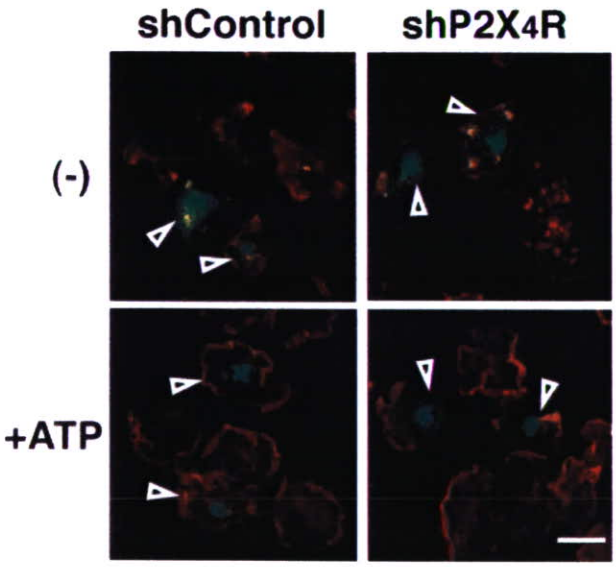

Fig. 9. Effect of P2X$_4$R downregulation on ATP-induced membrane ruffling of microglia. Microglia transduced with the lentivirus vectors were stimulated with 50 μM ATP for 5 min. After fixation, the cells were stained with Texas Red-conjugated phalloidin. Arrowheads indicate EGFP-positive cells. ATP-stimulated membrane ruffling of EGFP-positive cells were observed in three independent experiments. Scale bar, 20 μm.

ring (Vanhaesebroeck et al., 2001). When cells are placed in a chemoattractant gradient, the phosphorylated phospholipids selectively accumulate at the leading edge and act as a membrane anchor for many PI3K downstream effector proteins with pleckstrin homology (PH) regions, which may regulate directional sensing during chemotaxis (Procko and McColl, 2005; Van Haastert and Devreotes, 2004). PI3K will play a crucial role in both sensing the ATP gradient and determining the cell polarity of the microglia.

Akt is activated through binding of its PH domains to lipid products of PI3K on the plasma membrane (Scheid and Woodgett, 2003). In this study ATP-induced increase in Akt phosphorylation was suppressed by pretreatment with a P2Y$_{12}$R antagonist or PI3K inhibitors (Fig. 3). These findings indicated that Akt is phosphorylated following PI3K activation downstream of P2Y$_{12}$R in microglia. Interestingly, the increase in the Akt phosphorylation was suppressed by chelation of extracellular calcium with EGTA (Fig. 4), and depletion of intracellular calcium by BAPTA-AM also blocked the Akt phosphorylation (data not shown). These results indicate that activation of the PI3K-Akt signal pathway is regulated by an increase in $[Ca^{2+}]_i$. Previous studies have shown that in some cells an increase in $[Ca^{2+}]_i$ can activate Akt through PI3K-dependent or independent pathways. An increase in $[Ca^{2+}]_i$ can also activate Src or proline-rich/Ca^{2+}-activated tyrosine kinase Pyk2, thereby directly or indirectly regulating the PI3K activation (Chen et al., 2001; Gendron et al., 2003; Okuda et al., 1999). Protein kinase C (PKC) or Ca^{2+}/calmodulin-dependent protein kinase which is activated by calcium, lies upstream of Akt or directly phosphorylates Akt (Bauer et al., 2003; Gliki et al., 2002; Tanaka et al., 2003; Yano et al., 1998). Further investigation is needed to determine how the calcium signaling regulates the PI3K/Akt activation in microglia.

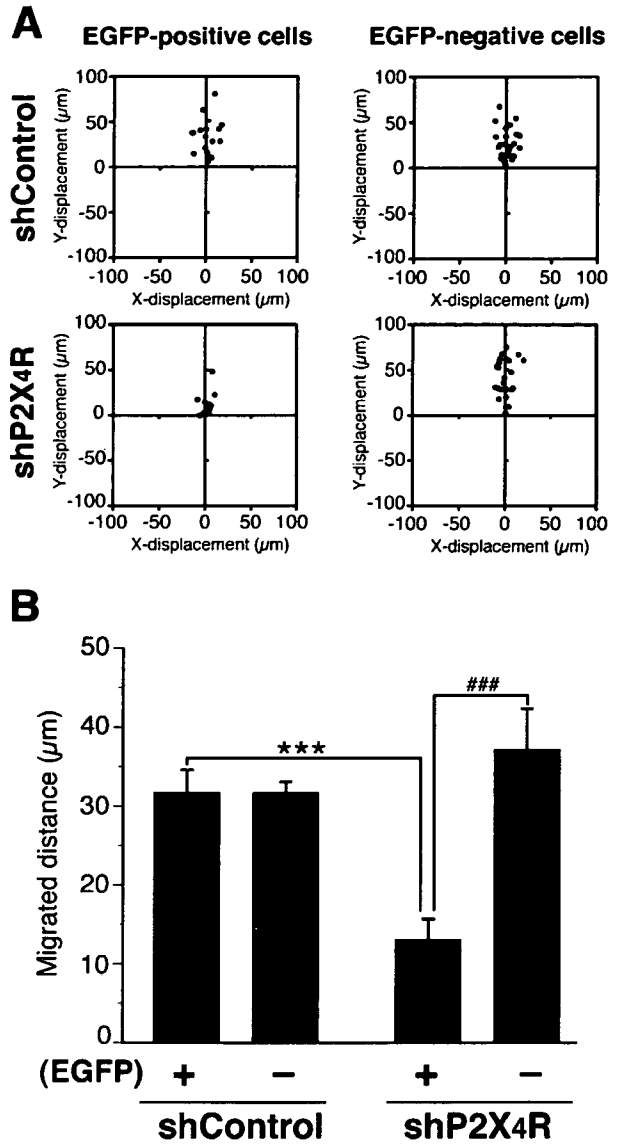

Fig. 10. Inhibitory effect of $P2X_4R$ downregulation on ATP-induced microglial chemotaxis. (**A**) Microglia were transduced with the lentivirus vectors and microglial migration towards 50 μM ATP was observed in the Dunn chemotaxis chamber. The distance and direction of movement by individual cells are shown as x and y coordinates on scatter diagrams. (**B**) Each chemotaxis was quantified by measuring the (x, y) distance migrated from the starting position of cells. Data are means ± SD of three independent experiments. $^{***}P < 0.001$, Student's t-test, compared with shControl EGFP-positive cells; $^{###}P < 0.001$, compared with shP2X4R EGFP-negative cells.

The ATP-induced increase in $[Ca^{2+}]_i$ in microglia has been shown to be suppressed by chelation of extracellular calcium or pretreatment with TNP-ATP, but not by PPADS or BBG (Tsuda et al., 2003). The present study showed that shRNA-mediated downregulation of $P2X_4R$ in microglia suppressed the ATP-induced increase in $[Ca^{2+}]_i$ (Fig. 8). These observations suggest that the increase in $[Ca^{2+}]_i$ is mainly caused by the influx of extracellular calcium through $P2X_4R$. ATP-induced PI3K/Akt activation was inhibited by pretreatment with TNP-ATP, but not with PPADS or BBG (Fig. 6). Interference with $P2X_4R$ expression markedly inhibited the ATP-induced microglial chemotaxis (Fig. 10) without affecting membrane ruffling (Fig. 9), the same as the effects of PI3K inhibitors (Figs. 1 and 2). We therefore suspect that the $P2X_4R$-mediated calcium signaling may be involved in PI3K/Akt activation and regulate microglial chemotaxis. Local Ca^{2+} mobilization through $P2X_4R$ at membrane ruffles may be necessary for maintenance or enhancement of the local $P2Y_{12}R$-activated PI3K signals.

Membrane ruffling is generated by dynamic remodeling of the actin cytoskeleton at the plasma membrane and is thought to be a crucial process for cell migration (Small et al., 2002). $P2Y_{12}R$ activation is essential for ATP-induced membrane ruffling and triggers intracellular signaling events that lead to microglial chemotaxis toward ATP. Ca^{2+} imaging showed that shP2×4R did not completely suppress the ATP-evoked increase in $[Ca^{2+}]_i$ (Fig. 9), suggesting that other subtypes of ATP receptor are involved in the Ca^{2+} response. P2Y receptors are generally linked to activation of phospholipase C (PLC) that catalyzes the hydrolysis of phosphatidylinositol 4,5-bisphosphate to the intracellular messenger inositol 1,4,5, triphosphate (IP_3) and diacylglycerol (Communi et al., 2000). ATP-stimulated $P2Y_{12}R$ will induce PLC activation, leading to IP_3-mediated Ca^{2+} release from intracellular calcium stores in microglia. P2Y receptors modulate G-protein coupled or voltage-dependent ion channels that affect the Ca^{2+} current (Van Kolen and Slegers, 2006). Vial et al. (2002) reported that coactivation of $P2X_1R$ and $P2Y_1R$ in platelets synergistically enhances the Ca^{2+} response and suggested that $P2X_1$ may have a priming role in the activation of $P2Y_1R$ during platelet activation. Further study is needed to analyze cross-talk between $P2X_4R$ and other signal pathways downstream of $P2Y_{12}R$, such as the adenylate cyclase pathway or PLC pathway.

$P2Y_{12}R$ is constitutively expressed in microglia in the normal brain (Sasaki et al., 2003). A recent report by Haynes et al. (2006) shows that $P2Y_{12}R$ is essential for early microglial responses towards either a local ATP injection or a focal laser injury in brain slices. $P2Y_{12}R$ play crucial roles in regulating the morphological changes in ramified microglia and cell migration by activated microglia in response to ATP released by surrounding cells and its hydrolysis product ADP. By contrast, $P2X_4R$ expression in microglia is lower in the normal brain and spinal cord, and it is significantly upregulated in activated microglia within 24 h after ischemia or nerve injury (Cavaliere et al., 2003; Schwab et al., 2005; Zhang et al., 2006). Tsuda et al. (2003) recently reported that the $P2X_4R$ expression is induced in spinal microglia during the tactile allodynia observed after nerve injury. These observations together with our own findings suggest that $P2X_4R$ activation may modulate or enhance the microglial cell migration in pathological conditions. Although further study is needed to clarify the molecular mechanisms underlying the microglial cell migration

mediated by P2Y$_{12}$R and P2X$_4$R, the findings in the present study may contribute to understanding the ATP-induced changes in microglial dynamics in the brain in normal and pathological states.

ACKNOWLEDGMENTS

We thank Dr. Miyoshi (Bio Resource Center, RIKEN, Tsukuba, Japan) for providing us with lentivirus vector system, and Dr. Shin'ichi Takeda, Dr. Hirohiko Hojoh, and Mr. Masuda Satoshi (National Institute of Neuroscience) for their advice and technical support.

REFERENCES

Bauer B, Jenny M, Fresser F, Uberall F, Baier G. 2003. AKT1/PKBα is recruited to lipid rafts and activated downstream of PKC isotypes in CD3-induced T cell signaling. FEBS Lett 541:155–162.

Bellacosa A, Testa JR, Staal SP, Tsichlis PN. 1991. A retroviral oncogene, akt, encoding a serine–threonine kinase containing an SH2-like region. Science 254:274–277.

Cavaliere F, Florenzano F, Amadio S, Fusco FR, Viscomi MT, D'Ambrosi N, Vacca F, Sancesario G, Bernardi G, Molinari M, Volonte C. 2003. Up-regulation of P2X$_2$, P2X$_4$ receptor and ischemic cell death: Prevention by P2 antagonists. Neuroscience 120:85–98.

Chen R, Kim O, Yang J, Sato K, Eisenmann KM, McCarthy J, Chen H, Qiu Y. 2001. Regulation of Akt/PKB activation by tyrosine phosphorylation. J Biol Chem 276:31858–31862.

Comalada M, Xaus J, Sanchez E, Valledor AF, Celada A. 2004. Macrophage colony-stimulating factor-, granulocyte–macrophage colony-stimulating factor-, or IL-3-dependent survival of macrophages, but not proliferation, requires the expression of p21(Waf1) through the phosphatidylinositol 3-kinase/Akt pathway. Eur J Immunol 34:2257–2267.

Communi D, Janssens R, Suarez-Huerta N, Robaye B, Boeynaems JM. 2000. Advances in signalling by extracellular nucleotides. The role and transduction mechanisms of P2Y receptors. Cell Signal 12:351–360.

Czajkowski R, Banachewicz W, Ilnytska O, Drobot LB, Baranska J. 2004. Differential effects of P2Y$_1$ and P2Y$_{12}$ nucleotide receptors on ERK1/ERK2 and phosphatidylinositol 3-kinase signalling and cell proliferation in serum-deprived and nonstarved glioma C6 cells. Br J Pharmacol 141:497–507.

Davalos D, Grutzendler J, Yang G, Kim JV, Zuo Y, Jung S, Littman DR, Dustin ML, Gan WB. 2005. ATP mediates rapid microglial response to local brain injury in vivo. Nat Neurosci 8:752–758.

Ferrari D, Villalba M, Chiozzi P, Falzoni S, Ricciardi-Castagnoli P, Di Virgilio F. 1996. Mouse microglial cells express a plasma membrane pore gated by extracellular ATP. J Immunol 156:1531–1539.

Gendron FP, Neary JT, Theiss PM, Sun GY, Gonzalez FA, Weisman GA. 2003. Mechanisms of P2X$_7$ receptor-mediated ERK1/2 phosphorylation in human astrocytoma cells. Am J Physiol Cell Physiol 284: C571–C581.

Gliki G, Wheeler-Jones C, Zachary I. 2002. Vascular endothelial growth factor induces protein kinase C (PKC)-dependent Akt/PKB activation and phosphatidylinositol 3′-kinase-mediates PKC δ phosphorylation: Role of PKC in angiogenesis. Cell Biol Int 26:751–759.

Haynes SE, Hollopeter G, Yang G, Kurpius D, Dailey ME, Gan WB, Julius D. 2006. The P2Y(12) receptor regulates microglial activation by extracellular nucleotides. Nat Neurosci 12:1512–1519.

Honda S, Sasaki Y, Ohsawa K, Imai Y, Nakamura Y, Inoue K, Kohsaka S. 2001. Extracellular ATP or ADP induce chemotaxis of cultured microglia through Gi/o-coupled P2Y receptors. J Neurosci 21:1975–1982.

Illes P, Alexandre Ribeiro J. 2004. Molecular physiology of P2 receptors in the central nervous system. Eur J Pharmacol 483:5–17.

Imai Y, Ibata I, Ito D, Ohsawa K, Kohsaka S. 1996. A novel gene iba1 in the major histocompatibility complex class III region encoding an EF hand protein expressed in a monocytic lineage. Biochem Biophys Res Commun 224:855–862.

Inoue K. 2002. Microglial activation by purines and pyrimidines. Glia 40:156–163.

Inoue K, Nakajima K, Morimoto T, Kikuchi Y, Koizumi S, Illes P, Kohsaka S. 1998. ATP stimulation of Ca^{2+}-dependent plasminogen release from cultured microglia. Br J Pharmacol 123:1304–1310.

Ito D, Imai Y, Ohsawa K, Nakajima K, Fukuuchi Y, Kohsaka S. 1998. Microglia-specific localisation of a novel calcium binding protein, Iba1. Brain Res Mol Brain Res 57:1–9.

James G, Butt AM. 2002. P2Y and P2X purinoceptor mediated Ca^{2+} signalling in glial cell pathology in the central nervous system. Eur J Pharmacol 447:247–260.

Kreutzberg GW. 1996. Microglia: A sensor for pathological events in the CNS. Trends Neurosci 19:312–318.

Moran LB, Graeber MB. 2004. The facial nerve axotomy model. Brain Res Brain Res Rev 44:154–178.

Nakajima K, Kohsaka S. 2005.Response of microglia to brain injury. In: Kettenmann H, Ransom BR, editors. Neuroglia. New York: Oxford University Press. pp 443–453.

Nakajima K, Shimojo M, Hamanoue M, Ishiura S, Sugita H, Kohsaka S. 1992. Identification of elastase as a secretory protease from cultured rat microglia. J Neurochem 58:1401–1408.

Nasu-Tada K, Koizumi S, Inoue K. 2005. Involvement of β1 integrin in microglial chemotaxis and proliferation on fibronectin: Different regulations by ADP through PKA. Glia 52:98–107.

Nimmerjahn A, Kirchhoff F, Helmchen F. 2005. Resting microglial cells are highly dynamic surveillants of brain parenchyma in vivo. Science 308:1314–1318.

Nishitsuji H, Ikeda T, Miyoshi H, Ohashi T, Kannagi M, Masuda T. 2004. Expression of small hairpin RNA by lentivirus-based vector confers efficient and stable gene-suppression of HIV-1 on human cells including primary non-dividing cells. Microbes Infect 6: 76–85.

Nörenberg W, Langosch JM, Gebicke-Haerter PJ, Illes P. 1994. Characterization and possible function of adenosine 5′-triphosphate receptors in activated rat microglia. Br J Pharmacol 111:942–950.

Okuda M, Takahashi M, Suero J, Murry CE, Traub O, Kawakatsu H, Berk BC. 1999. Shear stress stimulation of p130(cas) tyrosine phosphorylation requires calcium-dependent c-Src activation. J Biol Chem 274:26803–26809.

Procko E, McColl SR. 2005. Leukocytes on the move with phosphoinositide 3-kinase and its downstream effectors. Bioessays 27:153–163.

Ralevic V, Burnstock G. 1998. Receptors for purines and pyrimidines. Pharmacol Rev 50:413–492.

Ridley AJ. 2001. Rho proteins, PI 3-kinases, and monocyte/macrophage motility. FEBS Lett 498:168–171.

Sasaki Y, Hoshi M, Akazawa C, Nakamura Y, Tsuzuki H, Inoue K, Kohsaka S. 2003. Selective expression of Gi/o-coupled ATP receptor P2Y$_{12}$ in microglia in rat brain. Glia 44:242–250.

Scheid MP, Woodgett JR. 2003. Unravelling the activation mechanisms of protein kinase B/Akt. FEBS Lett 546:108–112.

Schwab JM, Guo L, Schluesener HJ. 2005. Spinal cord injury induces early and persistent lesional P2X$_4$ receptor expression. J Neuroimmunol 163:185–189.

Small JV, Stradal T, Vignal E, Rottner K. 2002. The lamellipodium: Where motility begins. Trends Cell Biol 12:112–120.

Soulet C, Sauzeau V, Plantavid M, Herbert JM, Pacaud P, Payrastre B, Savi P. 2004. Gi-dependent and -independent mechanisms downstream of the P2Y$_{12}$ ADP-receptor. J Thromb Haemost 2:135–146.

Stence N, Waite M, Dailey ME. 2001. Dynamics of microglial activation: A confocal time-lapse analysis in hippocampal slices. Glia 33:256–266.

Streit WJ. 2002. Microglia as neuroprotective, immunocompetent cells of the CNS. Glia 40:133–139.

Tanaka Y, Gavrielides MV, Mitsuuchi Y, Fujii T, Kazanietz MG. 2003. Protein kinase C promotes apoptosis in LNCaP prostate cancer cells through activation of p38 MAPK and inhibition of the Akt survival pathway. J Biol Chem 278:33753–33762.

Tsuda M, Shigemoto-Mogami Y, Koizumi S, Mizokoshi A, Kohsaka S, Salter MW, Inoue K. 2003. P2X$_4$ receptors induced in spinal microglia gate tactile allodynia after nerve injury. Nature 424:778–783.

Van Haastert PJ, Devreotes PN. 2004. Chemotaxis: Signalling the way forward. Nat Rev Mol Cell Biol 5:626–634.

Vanhaesebroeck B, Leevers SJ, Ahmadi K, Timms J, Katso R, Driscoll PC, Woscholski R, Parker PJ, Waterfield MD. 2001. Synthesis and function of 3-phosphorylated inositol lipids. Annu Rev Biochem 70:535–602.

Van Kolen K, Slegers H. 2004. P2Y$_{12}$ receptor stimulation inhibits β-adrenergic receptor-induced differentiation by reversing the cyclic AMP-dependent inhibition of protein kinase B. J Neurochem 89:442–453.

Van Kolen K, Slegers H. 2006. Integration of P2Y receptor-activated signal transduction pathways in G protein-dependent signaling networks. Purinergic Signalling 2:451–469.

Vial C, Rolf MG, Mahaut-Smith MP, Evans RJ. 2002. A study of P2X1 receptor function in murine megakaryocytes and human platelets reveals synergy with P2Y receptors. Br J Pharmacol 135:363–372.

Verkhratsky A, Kettenmann H. 1996. Calcium signalling in glial cells. Trends Neurosci 19:346–352.

Walz W, Ilschner S, Ohlemeyer C, Banati R, Kettenmann H. 1993. Extracellular ATP activates a cation conductance and a K^+ conductance in cultured microglial cells from mouse brain. J Neurosci 13:4403–4411.

Webb SE, Pollard JW, Jones GE. 1996. Direct observation and quantification of macrophage chemoattraction to the growth factor CSF-1. J Cell Sci 109:793–803.

Weiss-Haljiti C, Pasquali C, Ji H, Gillieron C, Chabert C, Curchod ML, Hirsch E, Ridley AJ, van Huijsduijnen RH, Camps M, Rommel C. 2004. Involvement of phosphoinositides 3-kinase γ, Rac, and PAK signaling in chemokine-induced macrophage migration. J Biol Chem 279:43273–43284.

Xiang Z, Burnstock G. 2005. Expression of P2X receptors on rat microglial cells during early development. Glia 52:119–126.

Yano S, Tokumitsu H, Soderling TR. 1998. Calcium promotes cell survival through CaM-K kinase activation of the protein-kinase-B pathway. Nature 396:584–587.

Yogosawa S, Hatakeyama S, Nakayama KI, Miyoshi H, Kohsaka S, Akazawa C. 2005. Ubiquitylation and degradation of serum-inducible kinase by hVPS18, a RING-H2 type ubiquitin ligase. J Biol Chem 280: 41619–41627.

Zhang Z, Artelt M, Burnet M, Trautmann K, Schluesener HJ. 2006. Lesional accumulation of $P2X_4$ receptor monocytes following experimental traumatic brain injury. Exp Neurol 197:252–257.

Vol 446|26 April 2007|doi:10.1038/nature05704

LETTERS

UDP acting at $P2Y_6$ receptors is a mediator of microglial phagocytosis

Schuichi Koizumi[1,2]*, Yukari Shigemoto-Mogami[1]*, Kaoru Nasu-Tada[1], Yoichi Shinozaki[1,3], Keiko Ohsawa[4], Makoto Tsuda[3], Bhalchandra V. Joshi[5], Kenneth A. Jacobson[5], Shinichi Kohsaka[4] & Kazuhide Inoue[3]

Microglia, brain immune cells, engage in the clearance of dead cells or dangerous debris, which is crucial to the maintenance of brain functions. When a neighbouring cell is injured, microglia move rapidly towards it or extend a process to engulf the injured cell. Because cells release or leak ATP when they are stimulated[1,2] or injured[3,4], extracellular nucleotides are thought to be involved in these events. In fact, ATP triggers a dynamic change in the motility of microglia *in vitro*[5,6] and *in vivo*[3,4], a previously unrecognized mechanism underlying microglial chemotaxis[5,6]; in contrast, microglial phagocytosis has received only limited attention. Here we show that microglia express the metabotropic $P2Y_6$ receptor whose activation by endogenous agonist UDP triggers microglial phagocytosis. UDP facilitated the uptake of microspheres in a $P2Y_6$-receptor-dependent manner, which was mimicked by the leakage of endogenous UDP when hippocampal neurons were damaged by kainic acid *in vivo* and *in vitro*. In addition, systemic administration of kainic acid in rats resulted in neuronal cell death in the hippocampal CA1 and CA3 regions, where increases in messenger RNA encoding $P2Y_6$ receptors that colocalized with activated microglia were observed. Thus, the $P2Y_6$ receptor is upregulated when neurons are damaged, and could function as a sensor for phagocytosis by sensing diffusible UDP signals, which is a previously unknown pathophysiological function of P2 receptors in microglia.

Microglia express several functional P2 receptors, and their $P2X_4$, $P2X_7$ and $P2Y_{12}$ receptors have already been described in relation to their physiological and pathophysiological consequences[5–9]. To investigate the expression of mRNAs for P2 receptors that are at a higher concentration in cultured rat microglia, we conducted reverse-transcriptase-mediated polymerase chain reaction (RT–PCR) analysis with complementary DNA coding for P2Y and P2X receptors (Fig. 1a). In accordance with previous reports[5–9], microglia expressed mRNAs encoding $P2X_4$, $P2X_7$ and $P2Y_{12}$ receptors. However, we found unexpectedly that cultured rat microglia expressed a large amount of mRNA coding for $P2Y_6$ receptors, which was also confirmed by western blotting for the expression of $P2Y_6$ receptor protein (Fig. 1b). The $P2Y_6$ receptor is coupled to the activation of phospholipase C (PLC), leading to the production of inositol 1,4,5-trisphosphate ($InsP_3$) and the release of Ca^{2+} from $InsP_3$-receptor-sensitive stores[10,11]. We therefore examined changes in the intracellular Ca^{2+} concentration ($[Ca^{2+}]_i$) in microglia and found that the $P2Y_6$ receptor agonist UDP evoked increases in $[Ca^{2+}]_i$ in a concentration-dependent manner, and it also increased the fraction of the UDP-responsive cells (Supplementary Fig. 1a). The elevations in $[Ca^{2+}]_i$ induced by 100 μM UDP were significantly inhibited by the PLC inhibitor U73122, the Ca^{2+}-ATPase inhibitor in sarcoplasmic/endoplasmic reticulum thapsigargin, and the membrane-permeable $InsP_3$ receptor inhibitor xestospongin C, but were little affected by pertussis toxin (Supplementary Fig. 1b). The UDP-evoked $[Ca^{2+}]_i$ increases in microglia were significantly inhibited by reactive blue 2 (RB2), known as a potent $P2Y_6$ antagonist[11], suramin, which inhibits $P2Y_6$ receptor at higher concentrations, the diisothiocyanate derivative MRS2578, which is a selective antagonist of the $P2Y_6$ receptor[12], and an antisense oligonucleotide (AS) for $P2Y_6$ receptors, but not by a random-sequence oligonucleotide (R-oligo) (Fig. 1c). All these data show that rat microglia express functional $P2Y_6$ receptors by which UDP mobilizes Ca^{2+}.

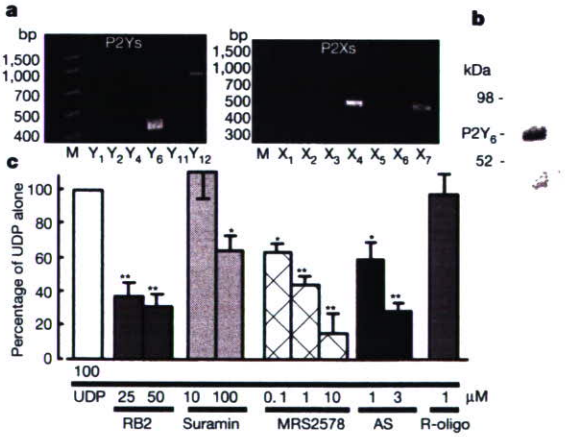

Figure 1 | Expression of $P2Y_6$ receptor and UDP-evoked increase in $[Ca^{2+}]_i$ in cultured microglia. a, RT–PCR analysis of the expression of mRNAs for $P2Y_6$, $P2Y_{12}$, $P2X_4$ and $P2X_7$ receptors in microglial cells. **b**, Expression of $P2Y_6$ receptor protein confirmed by western blotting analysis. **c**, Effects of various chemicals on the increase in $[Ca^{2+}]_i$ (measured as the change in ratio of fluorescence at 340 nm to that at 380 nm) evoked by 100 μM UDP in microglia. The maximum increase in Fura-2 fluorescence evoked by 100 μM UDP was considered as the control response, and values are expressed as a percentage of control. Data show means and s.e.m. for 24–36 cells obtained from at least three independent experiments. Significant differences from the response to UDP alone: asterisk, $P < 0.05$; two asterisks, $P < 0.01$ (Student's *t*-test).

[1]Division of Pharmacology, National Institute of Health Sciences, 1-18-1 Kamiyoga, Setagaya, Tokyo 158-8501, Japan. [2]Department of Pharmacology, Interdisciplinary Graduate School of Medicine and Engineering, University of Yamanashi, 1110 Shimokato, Chuo, Yamanashi 409-3893, Japan. [3]Department of Molecular and System Pharmacology, Graduate School of Pharmaceutical Sciences, Kyushu University, 3-1-1 Maidashi, Higashi, Fukuoka 812-8582, Japan. [4]Department of Neurochemistry, National Institute of Neuroscience, 4-1-1 Ogawahigashi, Kodaira, Tokyo 187-8502, Japan. [5]Molecular Recognition Section, Laboratory of Bioorganic Chemistry, National Institute of Diabetes and Digestive and Kidney Diseases, National Institutes of Health, Bethesda, Maryland 20892-0810, USA.
*These authors contributed equally to this work.

Morphogenesis, cell movement and phagocytosis are driven by dynamic reorganization of the actin cytoskeleton[13,14]. We showed previously that activation of $P2Y_{12/13}$ receptors, another microglial G-protein-coupled receptor, resulted in membrane ruffling and chemotaxis in microglia[5,6], and therefore we sought first to determine whether the $P2Y_6$-receptor-mediated signals affect the cell movement of microglia. Membrane ruffles are structures that are found primarily at the front edges of migrating cells[15]. To determine whether $P2Y_6$ activation stimulates microglial chemotaxis, cells were stimulated with either UDP or ATP. Neither lamellipodia-like membrane ruffles (Fig. 2a left) nor chemotaxis (Fig. 2b left) were observed when stimulated with UDP, whereas ATP produced both responses (Fig. 2a right and Fig. 2b right). However, UDP caused actin reorganization and formed aggregates of F-actin in the interior of the cells (Fig. 2a left, arrows). On stimulation with UDP (100 μM), microglia rapidly changed their morphology (Supplementary Fig. 2a); namely, to microglial processes with filopodia-like protrusions (arrows) and phagosome-like vacuoles (arrowheads). A crown-like circular structure rich in F-actins, termed the 'phagocytotic cup'[16], was also observed around the zymosan particles (Supplementary Fig. 2b, red). We speculated that UDP somehow regulates the morphogenesis of microglia, which may be involved in microglial endocytotic activities such as pinocytosis, macropinocytosis and phagocytosis. Phagocytosis is one of the most important physiological functions of microglia[17] and is the process activating the uptake of larger particles (more than 0.5 μm) by actin-based mechanisms. We investigated the UDP-evoked phagocytosis process by time-lapse videomicroscopy and flow cytometry (fluorescence-activated cell sorting; FACS)-based assay. When stimulated with 100 μM UDP, microglia rapidly phagocytosed fluorescent zymosan particles (green) (Fig. 2c, see also Supplementary Video). A quantitative phagocytosis assay by FACS shows that UDP induced the phagocytosis of latex beads in a concentration-dependent fashion (5–1,000 μM) in a 20-min incubation period (Fig. 2d). GDP (100–1,000 μM), a weak agonist of the $P2Y_6$ receptor, caused a slight uptake of microspheres (at 100 μM this was 49.7 ± 8.6% of UDP alone; $n = 4$) but ADP, also known as a weak partial agonist of the mouse $P2Y_6$ receptor, failed to stimulate the uptake (at 100 μM it was 0.3 ± 2.3% of UDP alone; $n = 4$). This is in good agreement with the previous finding that ADP does not activate rat $P2Y_6$ receptors[18]. The phagocytosis induced by 100 μM UDP was significantly inhibited by 30–100 μM RB2, a higher concentration of suramin (300 μM) and MRS2578 (0.01–3 μM), and was nearly abolished by $P2Y_6$ AS (Fig. 2e; see also Supplementary Fig. 2c, d). Recent reports indicate the existence of functional cross-talk between the nucleotides and cysteinyl leukotrienes (CysLTs, for example LTD4) in orchestrating inflammatory responses[19], indicating that some nucleotides may reveal their functions by means of a CysLT receptor (CysLTR). Microglia express a functional CysLT1R, whose activation by LTD4 resulted in an increase in $[Ca^{2+}]_i$ in microglia (Supplementary Fig. 3a). Thus, UDP acting on CysLT1R may reveal various microglial responses. However, MRS2578, a selective $P2Y_6$ receptor antagonist, did not block the LTD4-evoked Ca^{2+} responses in CysLT1R-transfected Chinese hamster ovary cells (Supplementary Fig. 3b) at a dose that inhibited the UDP-evoked increase in $[Ca^{2+}]_i$ and phagocytosis in microglia (Figs 1c and 2e). In addition, 1 μM LTD4 did not induce phagocytosis in microglia (Supplementary Fig. 3c, 4.8 ± 4.2% of that with 100 μM UDP alone; $n = 3$). All these findings suggest that the contribution of the CysLT1R to the UDP-evoked phagocytosis in microglia is negligible. Taken together, these data strongly suggest that rat microglial $P2Y_6$ receptors are coupled with phagocytic functions. The UDP-evoked phagocytosis was inhibited by 1 μM thapsigargin, the protein kinase C inhibitor staurosporin at 5 μM, and 10 μM U73122 (see Supplementary Fig. 4), indicating that activation of the $P2Y_6$ receptor seems to trigger phagocytosis through the pathway(s) mediated by PLC-linked Ca^{2+} and protein kinase C.

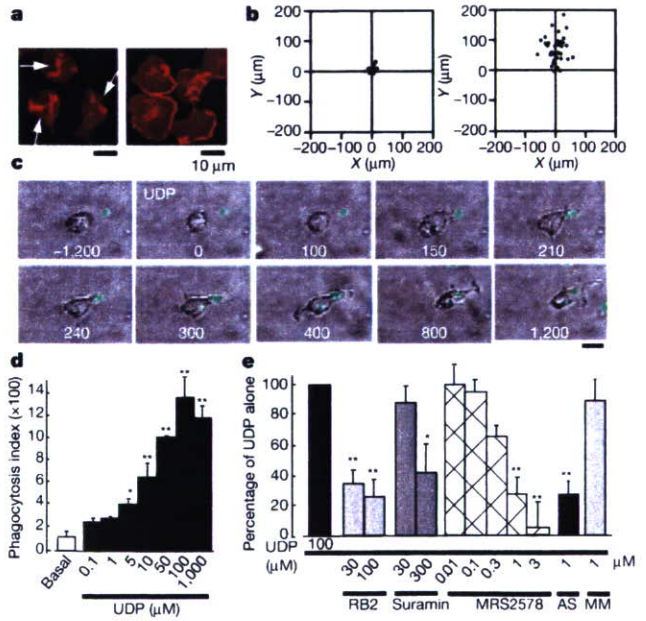

Figure 2 | Changes in cell motilities of microglia. **a**, UDP- and ATP-evoked membrane ruffles. Cultured microglia were stimulated for 5 min with 100 μM UDP (left) and 10 μM ATP (right), fixed, permeabilized, and then stained with anti-phalloidin. Scale bar, 10 μm. **b**, Typical chemotactic responses of microglia towards 100 μM UDP (left) and 100 μM ATP (right) assessed by the Dunn chemotaxis chamber (see Methods). **c**, Time-lapse images showing the effect of UDP on the microglial morphogenic changes and the uptake of fluorescent zymosan particles (green). The time after addition of UDP is shown in seconds in each picture. **d**, The UDP-evoked uptake of microspheres was assessed quantitatively as a phagocytosis index by using FACS. Data are mean and s.e.m. for three experiments (asterisk, $P < 0.05$; two asterisks, $P < 0.01$ compared with basal). **e**, Effects of the P2 receptor antagonists reactive blue 2 and suramin, the $P2Y_6$ receptor antagonist MRS2578, and $P2Y_6$ AS or MM on the UDP-evoked phagocytosis. Data are means and s.e.m. for three or four experiments (asterisk, $P < 0.05$; two asterisks, $P < 0.01$ compared with UDP alone).

Because phagocytes remove dead or damaged cells, debris and invading pathogens, recognition is the first step in phagocytosis. It is initiated by activation of the phagocytosis-promoting receptors such as Fc receptors and complement receptors[20]. In the central nervous system, microglia possess these receptors and remove amyloid-β, a key molecule in Alzheimer's disease, and attenuate Alzheimer's disease-like pathology[21]. With regard to apoptotic cells, microglia may also remove such cells by recognizing so-called 'eat-me' signals[20]. However, in the present study we used non-opsonized zymosan (Fig. 2c) and latex beads (Fig. 2d, e), which were not recognized by opsonin-dependent receptors such as Fc receptors, complement receptors or vitronectin receptors. Phagocytosis-promoting receptors also include opsonin-independent ones such as β_1-integrins, mannose receptors, scavenger receptors and phosphatidylserine receptors[13]; in fact, microglia expressed all these receptors (Supplementary Fig. 5a–e, cell lysates). Among these receptors, β_1-integrin was detected as a bead-associated protein that was slightly increased on stimulation with UDP (Supplementary Fig. 5a, bead-associated) and localized at membrane ruffle-like or phagocytic cup-like structures (see also Supplementary Fig. 2b), to which fluorescent microspheres were attached (Supplementary Fig. 5f). However, we do not know whether β_1-integrin itself binds or recognizes the microspheres. β_1-Integrin might be involved in some way in the machinery of phagocytosis or in the uptake processes of the microspheres in response to UDP, but the precise target molecule or molecules that bind or recognize microspheres to be phagocytosed remains to be identified. The microglial phagocytosis seen in the present study is a new type that is promoted by the diffusible

extracellular molecule UDP. However, we cannot deny the possibility that the UDP may simply facilitate the machinery of phagocytosis and that UDP-evoked phagocytosis observed in this study may even include macropinocytosis.

To determine the expression and function of microglial $P2Y_6$ receptors *in vivo*, the excitotoxicity of brain injury was induced by kainic acid (KA) (Fig. 3). KA is an excitatory amino acid that is often used to cause limbic motor epilepsy or excitatory neuronal cell death *in vivo* and *in vitro*. KA acts on non-NMDA glutamate receptors to facilitate excess excitability, thereby leading to necrosis and even apoptosis of neurons. The hippocampal CA1 and CA3 regions are susceptible to neuronal death in response to KA[22]. When KA was injected intraperitoneally into rats (10 mg kg^{-1}), it produced typical limbic seizure within 60 min. At 72 h after the administration of KA, the brains were removed and were used for western blotting, immunohistochemical assays and *in situ* hybridization (ISH). Western blotting analysis showed that KA increased the expression of $P2Y_6$ receptors in comparison with the saline-injected control groups (Fig. 3A, B). Double staining of microglia and neurons by anti-Iba1 (green) and anti-neuronal nuclei (NeuN, red) antibodies, respectively, showed that KA induced severe neuronal loss in the hippocampal CA1 and CA3 regions, where intense Iba1-positive signals—indicative of microglia—were observed. KA increased the number of microglia appearing in the activated form with poorly ramified, short and thick processes (Fig. 3C, f–h). Small NeuN signals seemed to be incorporated in some microglia (see g and h in Fig. 3C), suggesting that microglia phagocytose damaged or dead neurons. These findings suggest that microglia might migrate or proliferate, probably as a result of KA-induced neuronal damage.

We further examined the cell types that produced increases in $P2Y_6$ receptor protein in response to the administration of KA, and found that $P2Y_6$ immunoreactivities (green in Fig. 3D) were associated with the microglia (OX-42, red in Fig. 3D, c) but not with astrocytes (glial fibrillary acidic protein (GFAP), red in Fig. 3D, d) or neurons (NeuN, red in Fig. 3D, e). Furthermore, we performed ISH to characterize the expression of mRNA coding for $P2Y_6$ receptors with the use of digoxigenin-labelled antisense RNA probe. Signals for $P2Y_6$ receptor mRNA were very low in the naive animals but were upregulated three days after treatment with KA (Fig. 3E, b; blue dots indicated by arrowheads). At this time, the number of microglia increased markedly, especially at the hippocampal CA3 and CA1 regions (Fig. 3C). After ISH, the sections were stained with anti-Iba1 antibody to characterize $P2Y_6$ receptor mRNA signals. In the hippocampal CA3 regions of naive rats, there were very few anti-Iba1-positive microglia that did not show $P2Y_6$ receptor mRNA. In contrast, in the hippocampal CA3 of KA-injected rats, there was an increased number of anti-Iba1-positive microglia, in which $P2Y_6$ receptor signals were colocalized with microglia (Fig. 3E, c; KA, black arrows, see also inset at higher magnification).

There is a growing literature about 'eat-me' signals that are expressed on the cell surface of apoptotic or dying cells. However, diffusible signals that trigger phagocytosis have received only limited attention. When neurons or cells are exposed to traumatic injury such as ischaemia, they swell and subsequently shrink as a result of

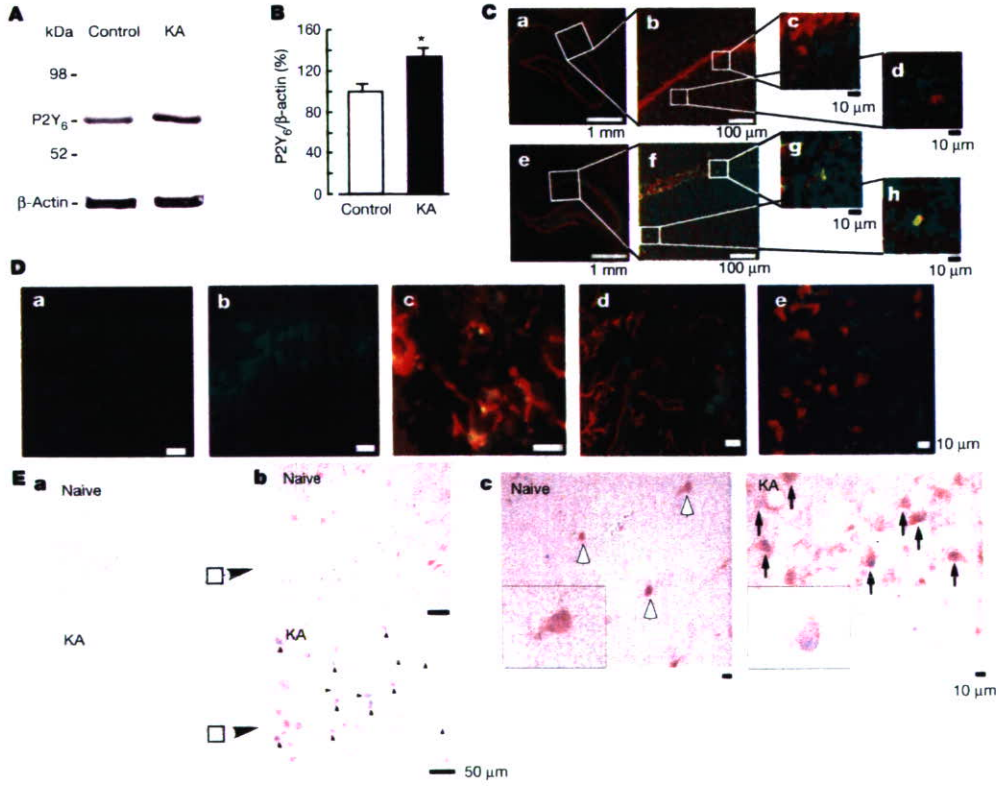

Figure 3 | Increase in $P2Y_6$ receptors in the hippocampus after kainic acid (KA)-treatment. A, Western blot analysis, showing increase in $P2Y_6$ receptor protein in rats treated intraperitoneally with 10 mg kg^{-1} KA, 72 h after treatment. **B**, Summary of quantitative data; KA was applied at 10 mg kg^{-1}. Results are means and s.e.m. for 8 (control) and 7 (KA) experiments (asterisk, $P < 0.05$ compared with control). **C**, Immunohistochemical analysis in naive control (**a**–**d**) and KA-treated (**e**–**h**) rats; red, anti-NeuN antibody; green, anti-Iba1 antibody. Rectangles in **a** and **e** are expanded in **b** and **f**, respectively. Rectangles in **b** and **f** also correspond to **c**, **d** and **g**, **h**, respectively. **D**, Anti-$P2Y_6$ antibody signals (green) were increased by KA (**a**, control; **b**, KA), which was colocalized with microglia (red in **c**, anti-OX42) but not with astrocytes (red in **d**, anti-GFAP) or neurons (red in **e**, anti-NeuN). **E**, ISH analysis. **a**, **b**, mRNA coding for $P2Y_6$ receptor in naive rats was very low but was increased at the hippocampal CA3 region by KA (3 days later) (blue dots and arrowheads, KA). **c**, Double staining with $P2Y_6$ antisense RNA probe (blue dots) and anti-Iba-1 antibody (brown signals, white (naive) or black (KA) arrows). In KA-treated rats there was an increased number of microglia, which was associated with $P2Y_6$ receptor mRNA (blue signals, inset at higher magnification in KA).

increased permeability. This is followed by leakage of cytoplasmic molecules, leading to necrotic cell death. Thus, cytoplasmic nucleotides could be diffusible messengers that signal the crisis state to adjacent cells including microglia. In fact, the diffusible messenger ATP promotes microglial chemotaxis and/or migration[3–6]. Diffusible molecules might be insufficiently precise to cause phagocytes to recognize and eat cells. However, released or leaked nucleotides are immediately degraded by the extracellular nucleotide-degrading enzymes. In this respect, UDP might be a localized and transient marker of traumatized or necrotic cells.

Cell injury results in a leakage of ATP that affects the motility of adjacent cells, including microglia[3,4]. In addition, cells release or leak uridine nucleotides[23] and nucleotide sugars[24] in response to various stimuli or ischaemic injury[25]. We therefore next investigated whether KA increases the release of extracellular UDP from neurons to induce microglial phagocytosis. Cultured hippocampal neurons were stimulated with and without 100 μM KA for 1 h; the supernatant was then collected for nucleotide assay by high-performance liquid chromatography (HPLC) or for phagocytosis assay by FACS (Fig. 4). Because released or leaked UTP is rapidly degraded into UDP, UMP and uridine by ARL67156-sensitive ectonucleotidases, we monitored the amount of UTP rather than UDP, and collected the supernatant and the microdialysates in the presence of 20 μM ARL67156 throughout experiments. There was a close relationship between the HPLC peak corresponding to UTP and the concentration of the standard UTP ($R^2 = 0.9947$). The amount of UTP in the KA-treated supernatant was significantly larger than that in the KA-untreated control supernatant (Fig. 4b; control, 2.3 ± 1.1 μM; KA treated, 10.5 ± 3.9 μM, $P < 0.05$). We also tested whether the KA-treated supernatant obtained from cultured hippocampal neurons facilitated microglial phagocytosis. Hippocampal neurons were treated with and without 100 μM KA for 1 h; each supernatant was collected and added to microglia; this was followed by a phagocytosis assay. As shown in Fig. 4c, when microglia were incubated with the KA-treated supernatant for 20 min, there was a significant increase in phagocytosis, which was blocked by the $P2Y_6$ receptor antagonist MRS2578 (1 μM). KA alone did not stimulate phagocytosis.

Finally, we tested whether KA induces the release of UDP and $P2Y_6$-receptor-mediated phagocytosis *in vivo*. An increase in extracellular UTP concentration ($[UTP]_o$) was observed soon after injection of KA (from 1 to 4 h after injection), which reached 2–3-fold higher than the KA-untreated control (data not shown). At 1 day after KA injection, $[UTP]_o$ was about 1.5–2.0-fold higher than the KA-untreated control (Fig. 4e). Then, at day 3, $[UTP]_o$ reached almost 10-fold higher levels (9.4 ± 1.2-fold; Fig. 4e and inset), which decreased slightly at day 5. A higher (5–10-fold) $[UTP]_o$ was observed 2–3 days after the injection of KA, which lasted at least another couple of days. It should be noted that loss of neurons (removal of neurons) also became obvious 2–3 days after the KA injection. We further injected fluorescent microspheres into the hippocampal CA3 regions of KA-treated rats, and then counted the numbers of the microspheres phagocytosed or attached by microglia. The $P2Y_6$ receptor antagonist MRS2578 was injected into the hippocampal CA3 region, and $P2Y_6$ AS or MM (mismatch oligonucleotide) was injected into the third ventricle. The number of microspheres taken or attached by microglia was markedly increased by KA treatment, which is significantly inhibited by MRS2578 or $P2Y_6$ AS but not by MM (Fig. 4g; see also Supplementary Fig. 6). These findings all suggest that UDP/$P2Y_6$-receptor-mediated signals are important for microglial phagocytosis even *in vivo*.

A recent review described that dying cells use both 'find-me' and 'eat-me' signals for phagocyte attraction and recognition[26]. Nucleotides could be both 'find-me' and 'eat-me' signals. The intracellular ATP concentration is estimated to be high (more than 5 mM) and the UTP concentration is reported to be one-third that of ATP[23]. Cells release ATP, and here we showed that KA caused an increase in extracellular UTP or UDP. Microglia might therefore be attracted by ATP or ADP[5,6] and subsequently recognize UDP, leading to the removal of the dying cells or their debris. It is interesting that ATP/ADP is not able to efficiently activate $P2Y_6$ receptors; neither can UDP act on $P2Y_{12/13}$ receptors. Thus, even if these nucleotides were leaked or released simultaneously, adenine and uridine nucleotides would regulate microglial motilities, namely chemotaxis and phagocytosis, in a mutually exclusive but coordinated fashion.

So far we have not shown quantitative data indicating that individual microglia upregulate the expression of $P2Y_6$ receptors. A significant, but not drastic, increase in $P2Y_6$ receptor protein in the hippocampus was observed after injection of KA (Fig. 3A, B). ISH data show that expression of mRNA coding for $P2Y_6$ receptors in microglia was very low in naive animals but became obvious in an increased number of microglia after KA injection (Fig. 3E), suggesting that the increase in $P2Y_6$ receptor protein is not due simply to an increased number of microglia but is upregulated in individual

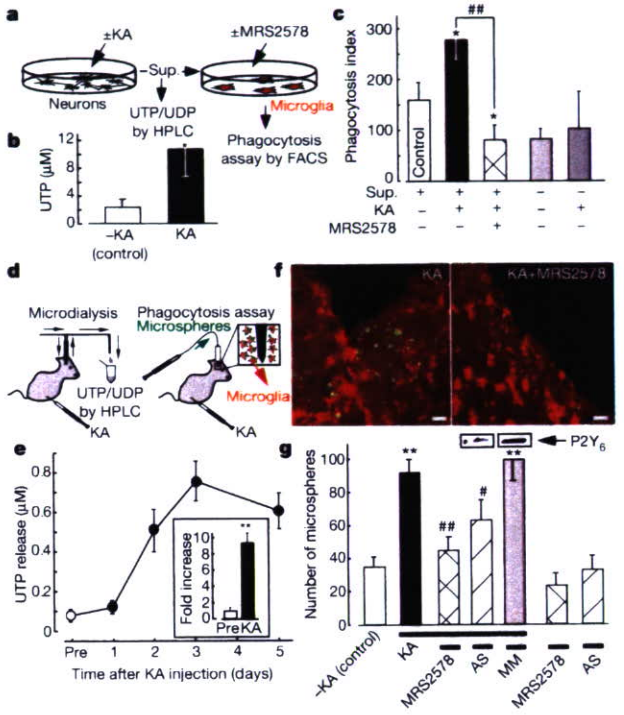

Figure 4 | KA-evoked increases in extracellular uridine nucleotides and $P2Y_6$-receptor-mediated microglial phagocytosis *in vitro* and *in vivo*. **a**, Schematic diagram of the experiments *in vitro*. Sup., supernatant. **b**, Summary of the UTP concentration in the KA-treated and control supernatants. Data show means and s.e.m. for at least five independent experiments (asterisk, $P < 0.05$ compared with control). **c**, Effects of the KA-treated and control supernatant on microglial uptake of fluorescent latex beads. Data show means and s.e.m. for at least four independent experiments (asterisk, $P < 0.05$ compared with control; hash sign, $P < 0.05$ compared with KA-treated supernatant). **d**, Schematic diagram of the experiments *in vivo*. KA was applied intraperitoneally at 10 mg kg^{-1}. **e**, Time course of changes in $[UTP]_o$ in baseline dialysates (before treatment with KA (Pre), and 1, 2, 3 and 5 days afterwards). Inset, fold increase at day 3 (compared with before treatment). **f**, Typical pictures of fluorescent microspheres (green) attached or taken up by microglia (red, anti-Iba1) in the KA-treated (left) and KA + MRS2578-treated (right) hippocampal CA3 regions. Scale bar, 20 μm. **g**, Quantitative analysis of phagocytosis *in vivo* (details are provided in Supplementary Methods). Changes in $P2Y_6$ receptor protein by $P2Y_6$ AS or MM are shown at the top of corresponding columns. Values are means and s.e.m. (asterisk, $P < 0.01$ compared with control (−KA); hash sign, $P < 0.05$; two hash signs, $P < 0.01$ compared with KA-treated group). Statistical analyses were performed by ANOVA with Scheffe's multiple comparison. At least three sections containing the injection sites were analysed per animal, and at least three animals were used in each group for analysis.

microglia. We also emphasize that even if the extent of $P2Y_6$ receptor upregulation is not drastic, an increase in extracellular UDP, a ligand for $P2Y_6$ receptor, is markedly increased after treatment with KA (detected as UTP, almost 10-fold; Fig. 4e) and therefore that the UDP/$P2Y_6$ receptor system would be sufficiently activated to cause microglial phagocytosis after treatment with KA. In comparison with the extensive knowledge of the molecular events involved in the regulation of apoptosis or necrosis, relatively little is known about the processes responsible for the clearance of dead cells and the degradation of waste materials. Considering the present findings that injured neurons leak diffusible UTP/UDP and cause the upregulation of $P2Y_6$ receptors in microglia, the UDP/$P2Y_6$ receptor system might function as a critical device covering the phagocytosis of both apoptotic and necrotic cells if they release or leak UDP by sensing diffusible UDP signals.

Thus we have shown that microglia express $P2Y_6$ receptors that function as a sensor of phagocytosis. The $P2Y_6$ receptor agonist UDP is released (as UTP) when neurons are damaged by KA. Thus, the activation of $P2Y_6$ receptors by UDP would be a key event in initiating the clearance of dying cells or debris in the central nervous system.

METHODS

Detailed methods are provided in Supplementary Information.

Microglia culture. The protocol was reviewed and approved by the Committee for Institutional Laboratory Animal Care of the National Institute of Health Sciences. Rat primary cultured microglia were prepared in accordance with the method described previously[27].

Phagocytosis assay *in vitro* and *in vivo*. *In vitro* microglial phagocytosis was assessed by either FACScan analysis or imaging analysis with fluorescently labelled microspheres. For the *in vivo* phagocytosis assay, fluorescently labelled microspheres were injected into the hippocampal CA3 region after injection of KA, and then the number of fluorescent microspheres associated with microglia was analysed by confocal microscopy (LSM 5 Pascal; Carl Zeiss).

Microdialysis. A microdialysis probe (A-I type probe; Eicom) was inserted into the hippocampal CA3 region by means of a guide cannula, and was perfused continuously at a flow rate of 3.0 μl min^{-1} (collected for 60 min) supplemented with the ectonuclease inhibitor ARL67156 (20 μM) (Sigma).

Quantification of UTP by HPLC. The concentration of nucleotides in the supernatant of the hippocampal cultures was analysed with an HPLC system (Jasco) combined with a C_{18} column (4.6 × 250 mm, Shodex) as described[28], with minor modifications.

Data analysis and statistics. All results are expressed as means ± s.e.m. A statistical analysis was performed with Student's *t*-test or analysis of variance, followed by Scheffe's multiple comparison test. Differences were considered to be significant at $P < 0.05$.

Received 23 December 2006; accepted 23 February 2007.
Published online 4 April 2007.

1. Guthrie, P. B. *et al.* ATP released from astrocytes mediates glial calcium waves. *J. Neurosci.* 19, 520-528 (1999).
2. Koizumi, S., Fujishita, K., Tsuda, M., Shigemoto-Mogami, Y. & Inoue, K. Dynamic inhibition of excitatory synaptic transmission by astrocyte-derived ATP in hippocampal cultures. *Proc. Natl Acad. Sci. USA* 100, 11023-11028 (2003).
3. Nimmerjahn, A., Kirchhoff, F. & Helmchen, F. Resting microglial cells are highly dynamic surveillants of brain parenchyma *in vivo*. *Science* 308, 1314-1318 (2005).
4. Davalos, D. *et al.* ATP mediates rapid microglial response to local brain injury *in vivo*. *Nature Neurosci.* 8, 752-758 (2005).
5. Honda, S. *et al.* Extracellular ATP or ADP induce chemotaxis of cultured microglia through $G_{i/o}$-coupled P2Y receptors. *J. Neurosci.* 21, 1975-1982 (2001).
6. Nasu-Tada, K., Koizumi, S. & Inoue, K. Involvement of β1 integrin in microglial chemotaxis and proliferation on fibronectin: different regulations by ADP through PKA. *Glia* 52, 98-107 (2005).
7. Ferrari, D. *et al.* P2Z purinoreceptor ligation induces activation of caspases with distinct roles in apoptotic and necrotic alterations of cell death. *FEBS Lett.* 447, 71-75 (1999).
8. Suzuki, T. *et al.* Production and release of neuroprotective tumor necrosis factor by P2X7 receptor-activated microglia. *J. Neurosci.* 24, 1-7 (2004).
9. Tsuda, M. *et al.* P2X4 receptors induced in spinal microglia gate tactile allodynia after nerve injury. *Nature* 424, 778-783 (2003).
10. Chang, K., Hanaoka, K., Kumada, M. & Takuwa, Y. Molecular cloning and functional analysis of a novel P2 nucleotide receptor. *J. Biol. Chem.* 270, 26152-26158 (1995).
11. Communi, D., Parmentier, M. & Boeynaems, J. M. Cloning, functional expression and tissue distribution of the human P2Y6 receptor. *Biochem. Biophys. Res. Commun.* 222, 303-308 (1996).
12. Mamedova, L. K., Joshi, B. V., Gao, Z. G., von Kugelgen, I. & Jacobson, K. A. Diisothiocyanate derivatives as potent, insurmountable antagonists of P2Y6 nucleotide receptors. *Biochem. Pharmacol.* 67, 1763-1770 (2004).
13. Greenberg, S. Signal transduction of phagocytosis. *Trends Cell Biol.* 5, 93-99 (1995).
14. Mitchison, T. J. & Cramer, L. P. Actin-based cell motility and cell locomotion. *Cell* 84, 371-379 (1996).
15. Lauffenburger, D. A. & Horwitz, A. F. Cell migration: a physically integrated molecular process. *Cell* 84, 359-369 (1996).
16. Ohsawa, K., Imai, Y., Kanazawa, H., Sasaki, Y. & Kohsaka, S. Involvement of Iba1 in membrane ruffling and phagocytosis of macrophages/microglia. *J. Cell Sci.* 113, 3073-3084 (2000).
17. Kreutzberg, G. W. Microglia: a sensor for pathological events in the CNS. *Trends Neurosci.* 19, 312-318 (1996).
18. Nicholas, R. A. *et al.* Pharmacological and second messenger signalling selectivities of cloned P2Y receptors. *J. Auton. Pharmacol.* 16, 319-323 (1996).
19. Mellor, E. A., Maekawa, A., Austen, K. F. & Boyce, J. A. Cysteinyl leukotriene receptor 1 is also a pyrimidinergic receptor and is expressed by human mast cells. *Proc. Natl Acad. Sci. USA* 98, 7964-7969 (2001).
20. Lauber, K. *et al.* Apoptotic cells induce migration of phagocytes via caspase-3-mediated release of a lipid attraction signal. *Cell* 113, 717-730 (2003).
21. Bard, F. *et al.* Peripherally administered antibodies against amyloid β-peptide enter the central nervous system and reduce pathology in a mouse model of Alzheimer disease. *Nature Med.* 6, 916-919 (2000).
22. Sperk, G. *et al.* Kainic acid induced seizures: neurochemical and histopathological changes. *Neuroscience* 10, 1301-1315 (1983).
23. Lazarowski, E. R., Homolya, L., Boucher, R. C. & Harden, T. K. Direct demonstration of mechanically induced release of cellular UTP and its implication for uridine nucleotide receptor activation. *J. Biol. Chem.* 272, 24348-24354 (1997).
24. Lazarowski, E. R., Shea, D. A., Boucher, R. C. & Harden, T. K. Release of cellular UDP-glucose as a potential extracellular signaling molecule. *Mol. Pharmacol.* 63, 1190-1197 (2003).
25. Erlinge, D. *et al.* Uridine triphosphate (UTP) is released during cardiac ischemia. *Int. J. Cardiol.* 100, 427-433 (2005).
26. Ravichandran, K. S. 'Recruitment signals' from apoptotic cells: invitation to a quiet meal. *Cell* 113, 817-820 (2003).
27. Nakajima, K. *et al.* Identification of elastase as a secretory protease from cultured rat microglia. *J. Neurochem.* 58, 1401-1408 (1992).
28. Lazarowski, E. R., Boucher, R. C. & Harden, T. K. Constitutive release of ATP and evidence for major contribution of ecto-nucleotide pyrophosphatase and nucleoside diphosphokinase to extracellular nucleotide concentrations. *J. Biol. Chem.* 275, 31061-31068 (2000).

Supplementary Information is linked to the online version of the paper at www.nature.com/nature.

Acknowledgements We thank T. Shimizu and Dr. S. Ishii for providing CysLT1 receptor-expressed Chinese hamster ovary cells; K. Sakemi for technical assistance; Y. Sasaki for helpful suggestions; K. Suzuki and R. Adachi for allowing us to use the Pascal confocal microscope system; and T. Nishimaki-Mogami, Y. Ohno and T. Nagao for continuous encouragement. This study was supported in part by a grant from The National Institute of Biomedical Innovation, a grant from Uehara Memorial Foundation, a Grant-in-Aid for Scientific Research on Priority Areas, for Creative Scientific Research, Scientific Research (A and B), and for Young Scientists (A) from the Ministry of Education, Science, Sports and Culture of Japan.

Author Contributions S.K. designed most experiments, performed Ca^{2+} imaging and *in vivo* experiments and wrote the paper. Y.S.M. conducted major parts of the experiments. K.N.T. and Y.S. carried out the FACS assay and the HPLC analysis, respectively. K.O. and S.K. performed the chemotaxis analysis. B.V.J. and K.A.J. made the $P2Y_6$ receptor antagonist MRS2578. M.T. analysed the data. K.I. analysed the data and coordinated the project. K.I. also designed the project. All authors discussed the results and commented on the manuscript.

Author Information Reprints and permissions information is available at www.nature.com/reprints. The authors declare no competing financial interests. Correspondence and requests for materials should be addressed to K.I. (inoue@phar.kyushu-u.ac.jp).

Available online at www.sciencedirect.com
ScienceDirect
Neurochemistry International 51 (2007) 105–111
NEUROCHEMISTRY International
www.elsevier.com/locate/neuint

Review

The functions of UCH-L1 and its relation to neurodegenerative diseases

Rieko Setsuie [a,b], Keiji Wada [a,*]

[a] *Department of Degenerative Neurological Diseases, National Institute of Neuroscience, National Center of Neurology and Psychiatry, Kodaira, Tokyo 187-8502, Japan*
[b] *Japan Health Sciences Foundation, Kyodo Building, 13-4 Kodenmacho, Nihonbashi, Chuo-ku, Tokyo 102-0001, Japan*

Received 31 March 2007; received in revised form 7 May 2007; accepted 9 May 2007
Available online 24 May 2007

Abstract

Parkinson's disease (PD) and Alzheimer's disease (AD), the most common neurodegenerative diseases, are caused by both genetic and environmental factors. Ubiquitin carboxy-terminal hydrolase L1 (UCH-L1) is a deubiquitinating enzyme that is involved in the pathogenesis of both of these neurodegenerative diseases. Several functions of UCH-L1, other than as an ubiquitin hydrolase, have been proposed; these include acting as an ubiquitin ligase and stabilizing mono-ubiquitin. This review focuses on recent findings on the functions and the regulation of UCH-L1, in particular those that relate to PD and AD.

Keywords: UCH-L1; Ubiquitin; Parkinson's disease; Alzheimer's disease; Gad mouse; Oxidative stress; Mono-ubiquitination

Contents

1. Introduction

Ubiquitin carboxy-terminal hydrolase L1 (UCH-L1), also known as PGP9.5, is a protein of 223 amino acids (Wilkinson et al., 1989). Although it was originally characterized as a deubiquitinating enzyme (Wilkinson et al., 1989), recent studies indicate that it also functions as a ubiquitin (Ub) ligase (Liu et al., 2002) and a mono-Ub stabilizer (Osaka et al., 2003). It is one of the most abundant proteins in the brain (1–2% of the total soluble protein) and immunohistochemical experiments demonstrate that it is exclusively localized in neurons (Wilson et al., 1988). Thus, its role in neuronal cell function/dysfunction was predicted. Indeed, the lack of UCH-L1 expression in mice results in gracile axonal dystrophy (*gad*) phenotype (Saigoh et al., 1999). Down-regulation and extensive oxidative modification of UCH-L1 have been observed in the brains of Alzheimer's disease (AD) patients as well as Parkinson's disease (PD) patients (Castegna et al., 2002; Choi et al., 2004; Butterfield et al., 2006). Moreover, administration of UCH-L1 was shown to alleviate the β-amyloid-induced synaptic dysfunction and memory loss associated with a mouse model of AD (Gong et al., 2006). In addition, an isoleucine 93 to

* Corresponding author. Tel.: +81 42 346 1715; fax: +81 42 346 1745.
E-mail address: wada@ncnp.go.jp (K. Wada).

0197-0186/$ – see front matter © 2007 Elsevier Ltd. All rights reserved.
doi:10.1016/j.neuint.2007.05.007

methionine amino acid mutation (I93M) of UCH-L1 was identified as a cause of autosomal dominant PD (Leroy et al., 1998). Our recent analysis of transgenic (Tg) mice expressing UCH-L1^{I93M}, showed an age-dependent loss of dopaminergic neurons, which is one of the pathological hallmarks of PD (Setsuie et al., 2007). On the contrary, a polymorphism that results in the amino acid substitution of serine 18 to tyrosine in UCH-L1 (UCH-L1^{S18Y}) was linked to decreased susceptibility to PD in some populations (Maraganore et al., 1999; Wintermeyer et al., 2000; Wang et al., 2002; Elbaz et al., 2003; Toda et al., 2003; Maraganore et al., 2004; Facheris et al., 2005; Tan et al., 2006; Carmine Belin et al., 2007). Together, all of these aspects indicate that the precise regulation of UCH-L1 is essential for neurons to survive and to maintain their proper function. In this review, we would like to summarize recent findings on UCH-L1, mostly those that relate to PD and AD.

2. The molecular functions of UCH-L1

UCH-L1 was first discovered as a member of the ubiquitin carboxy-terminal hydrolase family of deubiquitinating enzymes (Wilkinson et al., 1989; Nijman et al., 2005). *In vitro* analysis indicated that UCH-L1 can hydrolyze bonds between Ub and small adducts or unfolded polypeptides (Fig. 1). It can also cleave Ub gene products, either tandemly conjugated Ub monomers (UbB, UbC) or Ub fused to small ribosomal protein (S27a), very slowly, to yield free Ub, *in vitro* (Fig. 1) (Larsen et al., 1998). However, all of the activities detected *in vitro* are significantly lower than those of any other known Ub hydrolases, and its *in vivo* substrate has not yet been identified. Indeed, X-ray crystallography analysis of UCH-L1 indicates that it might exist in an inactive form on its own, and binding partners that regulate its activity may be warranted (Das et al., 2006).

In 2002, a group identified another enzymatic activity in UCH-L1, Ub ligase activity, *in vitro* (Liu et al., 2002). UCH-L1 was shown to exhibit dimerization-dependent Ub ligase activity (Fig. 1). Thus, from their observations, it is assumed that UCH-L1 might function as a hydrolase in a monomeric form and as a ligase in a dimeric form. Neither dimerization nor ligase activity were observed in the isozyme UCH-L3. In contrast to the well-recognized ubiquitination pathway (using E1, E2 and E3 ligases), which requires ATP to activate free Ub in order to conjugate Ub to the substrate, UCH-L1 does not require ATP, a notable characteristic of this ligase.

In addition, our group reported another function of UCH-L1, a mono-Ub stabilizing effect *in vivo*, which is independent of enzymatic activity (Osaka et al., 2003). We found that a large amount of mono-Ub is tightly associated with UCH-L1, inhibiting the degradation of mono-Ub in the brain. When UCH-L1 was over-expressed in SH-SY5Y cells, the half-life of mono-Ub was extended. Moreover, the expression level of UCH-L1 affected the level of mono-Ub in the mouse brain; *gad* mice showed a decreased level and UCH-L1^{WT} Tg mice showed an increased level of mono-Ub compared with wild-type mice. Thus, these results indicated that UCH-L1 functions as an Ub-stabilizing factor, regulating the pool size of mono-Ub *in vivo*

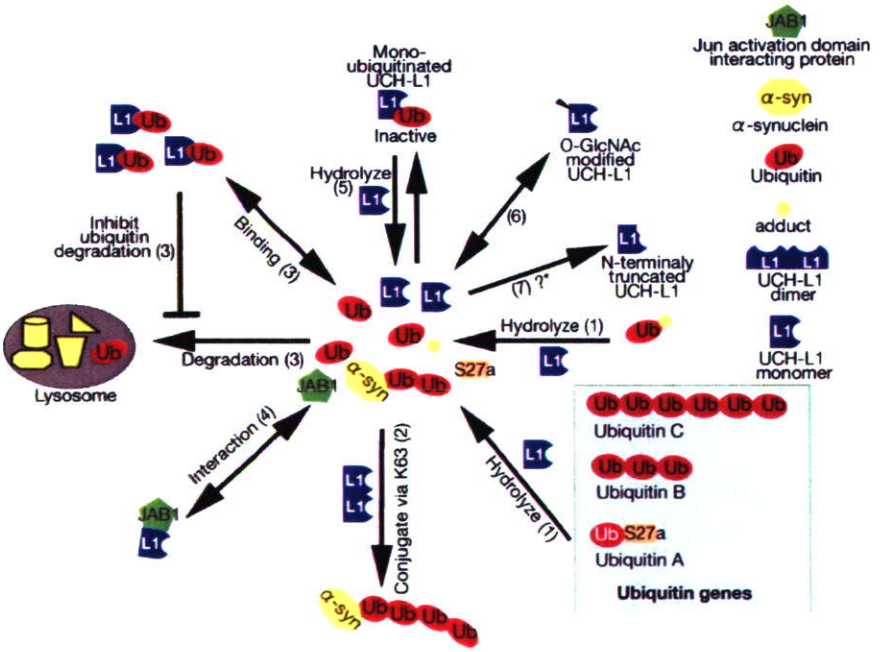

Fig. 1. Proposed functions and regulations of UCH-L1. (1) Under monomeric form, UCH-L1 can hydrolyze bond between Ub and small adduct or unfolded polypeptide *in vitro*. It can also cleave Ub gene products *in vitro*. (2) Under dimeric form, UCH-L1 ligase activity can produce K63 linked Ub chains to its substrate *in vitro*. One of its presumed substrate is di-ubiquitinated α-synuclein. (3) UCH-L1 is bound to mono-Ub *in vivo*. This interaction inhibits the degradation of mono-Ub. (4) UCH-L1 is shown to interact with Jun activation domain binding protein (JAB1). (5) Mono-ubiquitination and inactivation of UCH-L1 can occur reversibly. (6) *O*-GlcNAc-modified UCH-L1 is found in the synaptosome fraction. (7) N-terminally truncated forms of UCH-L1 are also found. *The truncated forms of UCH-L1 might occur as a result of either N-terminal processing of full length UCH-L1 or the translation from the different methionine. (8) The oxidatively modified UCH-L1 is also found in the diseased brains but is not shown in this figure. Please see the text for details.

(Fig. 1). Importantly, this mono-Ub stabilizing effect of UCH-L1 was independent of its enzymatic activity, as the C90S mutant, which lacks enzymatic activity but retains its Ub-interacting ability, still showed a mono-Ub stabilizing effect in cells.

As mentioned earlier, UCH-L1 is a highly expressed protein. Thus, the elucidation of the mechanisms involved in the regulation of UCH-L1 should be an important issue. Recently, a post-translational modification of UCH-L1 that controls the function of UCH-L1 was identified (Meray and Lansbury, 2007). The type of modification is mono-ubiquitination, which may occur reversibly to a lysine residue near the active site (probably K157) of UCH-L1 (Fig. 1). Mono-ubiquitinated UCH-L1, as mimicked by an Ub-UCH-L1 fusion protein, failed to bind mono-Ub and to increase mono-Ub levels in the cell. The enzymatic activity of UCH-L1 may also be inhibited by this modification because it prevents binding to the ubiquitinated targets. In addition, mono-ubiquitinated UCH-L1 was hydrolyzed in intra-molecular manner (Fig. 1). Thus, UCH-L1 might regulate its functional capability by auto-deubiquitination.

In addition to ubiquitination, the existence of a beta-*N*-acetylglucosamine (*O*-GlcNAc)-modified UCH-L1 in the synaptosome fraction of rat brain was reported (Fig. 1) (Cole and Hart, 2001). Moreover, amino-terminally truncated forms of UCH-L1 were found in human brains (Fig. 1), and the levels of this truncated form were shown to be decreased in AD brains but not in PD brains (Choi et al., 2004). Further effort to elucidate the physiological significance of these modifications and their relationship to the pathogenesis of AD and PD should be made.

3. *Gad* mice and the physiological function of UCH-L1 in the brain

Gad mice exhibit an autosomal recessively inherited disorder caused by an in-frame deletion that includes exons 7 and 8 of *Uchl1*, leading to a lack of UCH-L1 expression (Saigoh et al., 1999). These mice show sensory ataxia at an early stage, followed by motor ataxia at a later stage. Pathologically, the mutant is characterized by 'dying-back'-type axonal degeneration and formation of spheroid bodies in nerve terminals. In addition, *gad* mice show abnormal accumulation of APP, β-amyloid (Ichihara et al., 1995), Ub, and proteasome subunit-positive deposits (Saigoh et al., 1999) in the degenerating neuronal axons. These results clearly indicate that UCH-L1 is essential for the functional maintenance of some subsets of neuronal axons.

On the contrary, most neurons show no signs of degeneration in the brains of *gad* mice. By analyzing these neurons in *gad* mice, we found that a lack of UCH-L1 protects cells from acute stress-induced apoptosis (Harada et al., 2004). In wild-type mouse retina, light stimuli and ischemic retinal injury induced strong Ub expression in the inner retina with an expression pattern similar to that of UCH-L1. On the other hand, *gad* mice showed reduced Ub induction after light stimuli and ischemia, whereas the expression levels of anti-apoptotic and pro-survival proteins were significantly higher. Consistently, ischemia-induced caspase activity and neural cell apoptosis were suppressed to ~70% in *gad* mice. The heat-induced apoptosis of testicular cells was also suppressed in *gad* mice (Kwon et al., 2004). These reports demonstrate that UCH-L1 is involved in the regulation of stress-induced apoptosis, presumably through Ub induction.

4. Oxidative modification of UCH-L1 and neurodegeneration

Recently, an increased amount of oxidatively modified UCH-L1 in the brains of AD and PD patients, compared to normal brains, was reported (Castegna et al., 2002; Choi et al., 2004; Butterfield et al., 2006). The oxidative stress may cause such modifications to the protein. At present, several methionine residues and one cysteine residue of UCH-L1 have been reported as possible targets of oxidation; these form methionine sulfoxide and cysteinic acid (Cys–SO_3H), respectively, in PD and AD brains. Furthermore, the level of carbonyl-modified UCH-L1, which is also induced by oxidative stress, was found to be increased in PD and AD brains (Choi et al., 2004).

Consistent with the above data, addition of 4-hydroxy-2-nonenal (HNE; one of the carbonyls) induced the HNE modification of recombinant UCH-L1 *in vitro* (Nishikawa et al., 2003). HNE is an endogenous neurotoxin and a candidate mediator of oxidative stress caused by lipid hyperoxidation, known to trigger the cell death of neurons. In addition, proteins modified by HNE at lysine, histidine and/or cysteine residues are accumulated in the nigral neurons and the Lewy bodies of PD patients (Yoritaka et al., 1996; Castellani et al., 2002) and in the neurofibrillary tangles of AD patients (Montine et al., 1997). Cysteine (C90) and histidine (H161) form the active center of UCH-L1 along with asparagine (N176). Thus, the alteration of UCH-L1 activity was presumed to occur as a result of HNE modification. In agreement with this hypothesis, the hydrolase activities of HNE-modified UCH-L1 were reduced to about 40–80% of non-modified UCH-L1, and were inversely correlated with the degree of modification (Nishikawa et al., 2003). Oxidative stress is now recognized as an important factor, which is implicated in the pathogenesis of a number of age-related neurodegenerative diseases including PD and AD (Halliwell, 2006; Lin and Beal, 2006). Thus, the oxidative modification and subsequent decrease in the enzymatic activity of UCH-L1 may affect the function and survival of neurons, leading to the pathogenesis of AD and PD.

5. Decreased level of UCH-L1 and AD

As mentioned above, UCH-L1 is often present in the Ub-positive inclusions known as neurofibrillary tangles found in AD (Lowe et al., 1990). A recent report indicated that brains from patients with sporadic AD contain decreased levels of soluble UCH-L1, which is inversely proportional to tangle number (Choi et al., 2004). In addition, *gad* mice show an accumulation of amyloid precursor protein (APP) and β-amyloid, typical proteins accumulated in the inclusions of AD brains (Ichihara et al., 1995). Thus, a reduction in the levels of functional UCH-L1 was speculated to contribute to the

pathogenesis of AD. Recently, a group showed that the introduction of UCH-L1 rescued the synaptic and cognitive function of AD model mice (Gong et al., 2006). They used double Tg mice, over-expressing APP together with presenilin 1 (PS1), as an AD mouse model. At a young age following β-amyloid elevation, these mice showed cognitive defects such as inhibition of long-term potentiation (LTP), a type of synaptic plasticity related to memory. The protein level of UCH-L1 was significantly decreased in the hippocampi of these APP/PS1 Tg mice. Remarkably, synaptic function was restored to normal level when UCH-L1 protein fused to the transduction domain of HIV-transactivator protein (TAT) was transduced to hippocampal slices from APP/PS1 Tg mice. In fact, introduction of TAT-UCH-L1 to APP/PS1 mice, over time, improved their contextual learning. This therapeutic effect may be dependent on the enzymatic activity of UCH-L1 because the C90S mutant did not show any significant effect. These findings clearly demonstrate a link between decreased UCH-L1 function and the pathogenesis of AD. Further analysis may prove UCH-L1 to be a useful therapeutic target for treating AD.

6. I93M mutation with gain of toxic function of UCH-L1 and PD

In 1998, a cytosine to guanine (C277G) mutation in the *UCHL1* gene was reported in a German family affected with PD (Leroy et al., 1998). This missense mutation leads to an I93M amino acid substitution in the UCH-L1 protein. In this German family, four out of seven family members were affected with the autosomal dominant form of PD. All of the patients clinically resembled those with sporadic PD. However, there was an unaffected presumed carrier of this mutation in the family. Moreover, gene linkage analysis of *UCHL1* in other PD families failed to discover new families carrying this mutation. Therefore, the link between the I93M mutation in UCH-L1 and the development of PD has been questioned, with the assumption that the C277G alteration in the *UCHL1* gene is a rare polymorphism. To clarify the link between *UCHL1* mutation and PD, a series of experiments, including the *in vitro* biochemical analysis of mutant UCH-L1 and an analysis of Tg mice expressing UCH-L1^{I93M}, were performed.

The analysis of recombinant UCH-L1^{I93M} showed a decrease in its deubiquitinating activity to about 55% of the UCH-L1^{WT} activity level, using the model substrate Ub-amino methyl cumarine (AMC) (Table 1) (Leroy et al., 1998; Nishikawa et al., 2003). However, *gad* mice, which bear no activity of UCH-L1, show no signs of dopaminergic cell loss, the typical pathological hallmarks of PD. In addition, heterozygous mice, which are presumed to show half of the activity level seen in wild-type mice, are asymptomatic (Saigoh et al., 1999). Despite the species difference between mice and humans, these results indicate that the molecular mechanism involved in PD cannot simply be explained by decreased enzymatic activity (Saigoh et al., 1999).

We next compared the secondary structures of UCH-L1^{WT} and UCH-L1^{I93M} using recombinant proteins. Circular dichroism analysis showed that the UCH-L1^{I93M} contains a decreased level of α-helix compared with UCH-L1^{WT} (Table 1) (Nishikawa et al., 2003). It is reported that the SH-SY5Y cells expressing UCH-L1^{I93M} form an increased number of UCH-L1-positive aggregates compared with cells expressing UCH-L1^{WT} or UCH-L1^{C90S}, an enzymatic activity-defective mutant (Ardley et al., 2004). Thus, the I93M mutation may change the conformation of UCH-L1, leading to altered biochemical properties.

To ascertain if the I93M mutation gives rise to a gain of toxic function *in vivo*, we made a transgenic (Tg) mouse expressing UCH-L1^{I93M} (I93M Tg mouse) and analyzed this mouse to determine if UCH-L1^{I93M} could induce dopaminergic neuron loss. The I93M Tg mice showed several pathological changes related to PD (Setsuie et al., 2007). They showed an age-dependent decline in the number of tyrosine hydroxylase (TH)-positive dopaminergic neurons in the substantia nigra. The striatal dopamine content also decreased in parallel with the decrease in the number of dopaminergic neurons. Although we did not find any signs of Lewy body formation, we found silver staining-positive argyrophilic grains and abnormal electron dense core vesicles, which are also found in the autopsied brains of PD patients. In addition, we found aggregates containing both UCH-L1 and Ub in the perinuclei of dopaminergic neurons in the substantia nigra of I93M Tg mice. Therefore, the gain of toxic function caused by the I93M mutation in UCH-L1 might be the main factor contributing to the pathogenesis of PD.

Table 1
Association between UCH-L1 mutants and PD

	WT	I93M	S18Y	References
Incidence of PD		↑	↓	[a]
Functional comparison				
Hydrolase activity	(100%)	↓↓	↑	Leroy et al. (1998), Nishikawa et al. (2003)
Ligase activity	(100%)	↓	↓↓	Liu et al. (2002)
Mono-Ub binding affinity	+	ND	ND	Osaka et al. (2003)
Structural comparison				
α-Helix content	(Normal)	↓	±	Nishikawa et al. (2003), Naito et al. (2006)
Globularity[b]	+	+++	±	Naito et al. (2006)

[a] For references please see the text.
[b] The spherical shape is indicated as ± and the ellipsoidal degree is indicated by +.